

Two Component Singlet-Triplet Scalar Dark Matter and Electroweak Vacuum Stability

Amit Dutta Banik,^{1,*} Rishav Roshan,^{2,†} and Arunansu Sil^{2,‡}

¹*Key Laboratory of Quark and Lepton Physics (MoE) and Institute of Particle Physics,
Central China Normal University, Wuhan 430079, China*

²*Department of Physics, Indian Institute of Technology Guwahati, Assam-781039, India*

Abstract

We propose a two component dark matter setup by extending the Standard Model with a singlet and a hypercharge-less triplet scalars, each of them being odd under different Z_2 symmetries. We observe that the inter-conversion between the two dark matter components allow a viable parameter space where masses of both the dark matter candidates can be below TeV, even though their individual contribution to single component dark matter rules out any such sub-TeV dark matter. We find that a lighter mass of the neutral component of the scalar triplet, playing the role of one dark matter component, compared to the singlet one is favored. In addition, the setup is shown to make the electroweak vacuum absolutely stable till the Planck scale, thanks to Higgs portal coupling with the scalar dark matter components.

* amitdbanik@mail.ccnu.edu.cn

† rishav.roshan@iitg.ac.in

‡ asil@iitg.ac.in

I. INTRODUCTION

The Standard Model (SM) of particle physics undoubtedly emerges as the fundamental theory of interactions after discovery of the Higgs boson at the Large Hadron Collider (LHC) [1, 2]. However there still remains some issues, confirmed by experimental observations and can't be resolved within SM. For example, observation of cosmic microwave background radiation by Planck [3] reveals that about 26.5% of Universe is made up of mysterious dark matter (DM). The SM of particle physics, however, can not account for a dark matter candidate. Dark matter direct search experiments such as LUX [4], XENON-1T [5], PandaX-II [6, 7] search for the evidences of DM-nucleon interaction. Till date no such direct detection signal of DM has been detected which limits the DM-nucleon scattering cross-section. Apart from dark matter there also exists problem with the stability of electroweak (EW) vacuum within the Standard Model as the electroweak vacuum becomes unstable at large scale $\Lambda_I \sim 10^{10}$ GeV [8–12] for top quark mass $m_t = 173.2$ GeV [13]. This instability of EW vacuum at large scale can be restored in presence of additional scalars.

In order to address the above mentioned issues, we need to go beyond the SM. In this work, we will include new scalar particles which can serve as dark matter candidate and also stabilize the EW vacuum simultaneously. It is also to be noted that the null detection of DM in direct detection (DD) experiments also triggers the possibility of dark sector to be multi-component which is explored in many literatures in recent [14–41]. In multi-component dark matter scenario DM-DM conversion plays a significant role to determine the observables such as direct detection and relic density and also helps to stabilize EW vacuum with increased number of scalars. In this work, we consider a multi-component dark matter with scalar singlet and scalar triplet with zero hypercharge.

Study of scalar singlet dark matter and its effects on electroweak vacuum is done extensively in earlier works [42–53]. In a pure scalar singlet scenario, due to the presence of the quartic coupling between Higgs and dark matter can help Higgs quartic coupling become positive making the EW vacuum stable till Planck scale, M_{Pl} . It is found that singlet scalar with mass heavier than 900 GeV can satisfy the constraints coming from relic density, direct detection and vacuum stability [34]. Introducing an inert doublet as a possible dark matter component attracts a great amount of attention in recent days. It is found that there exists an intermediate region (80 - 500) GeV, beyond which the neutral component of the inert

Higgs satisfies the relic and DD constraints [54–65]. Recently it has been shown that in multi-component DM scenarios involving inert Higgs doublet(s) and/or singlet scalar, the region can be revived [33, 34].

Moving toward a further higher multiplet, it is found that an inert triplet can also be a possible dark matter candidate. A hypercharge-less ($Y=0$) inert triplet scalar can serve as a feasible dark matter candidate similar to inert Higgs doublet [54–67]. However, the allowed mass ranges of inert triplet dark matter is very much different from that of the inert doublet. Similar to the case of inert doublet, annihilation of triplet scalar is mostly gauge dominated which leaves a larger desert region compared to inert doublet. Also, due to small mass splitting between charged and neutral triplet scalar, co-annihilation channels into SM particles becomes relevant. Earlier studies [15, 68–71] reported that a pure inert triplet (with $Y=0$) dark matter, consistent with relic density, direct detection and vacuum stability constraints can be achieved with triplet mass ~ 1.9 TeV and triplet Higgs quartic coupling ~ 0.3 . In addition, the presence of the charge component in the scalar triplet also provides interesting discovery prospect in the collider searches [72]. The small mass splitting among the neutral and the charge component of the scalar triplet dictates the decay of the charged component only to the neutral component and to the soft pion or the soft lepton pairs and once produced these soft pions can lead to the disappearing charge track in the detector.

The other possibility is to have $Y = 2$ triplet scalar which is also investigated. It was shown in [68] that with $Y = 2$, dark matter mass $M_{\text{DM}} \geq 2.8$ TeV is allowed. For $Y = 2$ possibility, things are further restricted, mostly from the direct detection bounds. It is to be noted that unlike $Y = 2$ inert triplet scalar, neutral particles of $Y = 0$ inert triplet scalar does not have direct interaction with the Z boson which arise from the kinetic term in case of $Y = 2$ triplet. As a result, additional quark nucleon scattering via Z boson exchange occurs for $Y = 2$ inert triplet. This interaction term contributes to dark matter direct detection significantly and because of large scattering cross-section, most of the available parameter space is ruled out [68]. In this work we concentrate on $Y = 0$ triplet scalar.

As mentioned above, due to large gauge dominated annihilation, the relic density of $Y = 0$ inert triplet dark matter remains under-abundant up to ~ 1.8 TeV. Therefore, this leaves a great opportunity to explore the phenomenology of multi-component dark matter setup involving the inert triplet and a singlet scalars. Similar to the case of scalar singlet, the triplet Higgs quartic coupling also helps to stabilize the EW vacuum. In this work however,

we want to explore the below-TeV regime of both the dark matters in the two-component framework as this sub-TeV region is of great importance from the collider and dark matter experiments. In a work [15], although the authors explored a multi-component DM scenario with an inert triplet and a singlet scalars, the detailed effects of inter-conversion of DMs were not appropriately addressed in view of coupled Boltzmann equations. Furthermore, the work of [15] considered the results of DM direct detection experiments (*e.g.* XENON 100 data) which were not so stringent at the time of their analysis compared to the recent XENON 1T results. In our study however, we aim to show the pivotal importance of the conversion coupling in realizing the correct DM relic density by solving the coupled Boltzmann equations while taking into account the most recent DD experimental constraints into account. At the same time we also emphasise on the Higgs portal coupling of both the dark matters as they play a significant role in dark matter phenomenology and also in making the EW vacuum absolutely stable till M_{Pl} . We therefore search for a viable parameter space in this multi-component dark matter scenario that satisfies constraints from dark matter observables as well as electroweak vacuum stability can also be achieved.

The paper is organized as follows. The model is introduced in section II and the various theoretical and experimental constraints deemed relevant are detailed in section III. Section IV sheds light on the DM phenomenology. We then discuss the status of vacuum stability in V in this scenario and finally conclude in section VI.

II. MODEL

In the present setup, we extend the Standard Model particle content by introducing a $SU(2)_L$ triplet scalar T having hypercharge $Y = 0$ and a $SU(2)_L$ singlet scalar S . In addition, we include discrete symmetries $Z_2 \times Z'_2$ under which all the SM fields are even while additional fields transform differently. In Table I we provide the charge assignments of these additional fields under the SM gauge symmetry and the additional discrete symmetries imposed on the framework. Both the scalar singlet S and the neutral component of T can play the role of the dark matter candidates as they are charged odd under different Z_2 and hence stable. Therefore the present setup can accommodate a two-component dark matter scenario.

Particle	$SU(2)$	$U(1)_Y$	Z_2	Z'_2
H	2	$\frac{1}{2}$	+	+
T	3	0	-	+
S	1	0	+	-

TABLE I. Scalar particles and their charges under different symmetries.

The most general renormalisable scalar potential of our model, $V(H, T, S)$, consistent with $SU(2)_L \times U(1)_Y \times Z_2 \times Z'_2$ consists of (i) V_H : where sole contribution of the SM Higgs is included, (ii) V_T : involving contribution from scalar triplet T only, (iii) V_S : contribution of scalar singlet S only and (iv) V_{int} : specifying interactions among H , T , S . This is expressed as below:

$$V(H, T, S) = V_H + V_T + V_S + V_{int}. \quad (1)$$

where

$$V_H = -\mu_H^2 H^\dagger H + \lambda_H (H^\dagger H)^2, \quad (2a)$$

$$V_T = \frac{M_T^2}{2} \text{Tr}[T^2] + \frac{\lambda_T}{4!} (\text{Tr}[T^2])^2, \quad (2b)$$

$$V_S = \frac{M_S^2}{2} S^2 + \frac{\lambda_S}{4!} S^4, \quad (2c)$$

and

$$V_{int} = \frac{\lambda_{HT}}{2} (H^\dagger H) \text{Tr}[T^2] + \frac{\lambda_{HS}}{2} (H^\dagger H) S^2 + \frac{\kappa}{4} \text{Tr}[T^2] S^2. \quad (3)$$

In the above expression of Eq. (1), H denotes SM Higgs doublet. After the electroweak symmetry breaking (EWSB), the SM Higgs doublet obtains a vacuum expectation value (vev) $v = 246$ GeV. On the other hand, T^0 and S do not acquire any non-zero vacuum expectation value, thereby Z_2 and Z'_2 remains unbroken so as to guarantee the stability of the dark matter candidates.

The scalar fields can be parametrised as

$$H = \begin{pmatrix} w^+ \\ \frac{1}{\sqrt{2}}(v + h + iz) \end{pmatrix}, \quad T = \begin{pmatrix} \frac{1}{\sqrt{2}}T^0 & -T^+ \\ -T^- & -\frac{1}{\sqrt{2}}T^0 \end{pmatrix}, \quad S, \quad (4)$$

and after the EWSB, the masses of the physical scalars are given as

$$\begin{aligned} m_h^2 &= 2\lambda_H v^2, \\ m_{T^0, T^\pm}^2 &= M_T^2 + \frac{\lambda_{HT}}{2} v^2, \\ m_S^2 &= M_S^2 + \frac{\lambda_{HS}}{2} v^2. \end{aligned} \quad (5)$$

In Eq. (5), $m_h = 125.09$ GeV [73], is the mass of SM Higgs. It is to be noted that although mass of neutral and charged triplet scalar are degenerate, a small mass difference of Δm is generated via one loop correction [74, 75] and therefore T^0 can be treated as a stable DM candidate. This mass difference is expressed as

$$\Delta m = (m_{T^\pm} - m_{T^0})_{1-loop} = \frac{\alpha}{4\pi} m_{T^0} \left[f\left(\frac{M_W}{m_{T^0}}\right) - c_W^2 f\left(\frac{M_Z}{m_{T^0}}\right) \right], \quad (6)$$

where α is the fine structure constant, M_W , M_Z are the masses of the W and Z bosons, $c_W = \cos \theta_W = M_W/M_Z$ and $f(x) = -\frac{x}{4} \left[2x^3 \ln(x) + (x^2 - 4)^{3/2} \ln\left(\frac{x^2 - 2 - x\sqrt{x^2 - 4}}{2}\right) \right]$ where $x = \frac{M_{W,Z}}{m_{T^0}}$. It turns out that in the limit $x \rightarrow 0$ i.e. $m_{T^0} \gg M_W$ or M_Z , $f(x) \rightarrow 2\pi x$ and Δm can be expressed as [74]

$$\Delta m = \frac{\alpha}{2} M_W \sin^2 \frac{\theta_W}{2} \simeq 166 \text{ MeV}. \quad (7)$$

The couplings λ_{HS} and λ_{HT} denote the individual Higgs portal couplings of two DM candidates S and T^0 respectively whereas the coupling κ provides a portal which helps in converting one dark matter into another (depending on their mass hierarchy). For our analysis purpose, we first implement this model in LanHEP [76], choosing the independent parameters in the scalar sector as:

$$(m_{T^0}, m_S, \lambda_{HS}, \lambda_{HT}, \kappa).$$

III. THEORETICAL AND EXPERIMENTAL CONSTRAINTS

A. Theoretical constraints

The parameter space of this model is constrained by the theoretical consideration like the vacuum stability, perturbativity and unitarity of the scattering matrix. These constraints are as follows:

- (i) **Stability:** Due to the presence of extra scalars (T and S) in our model, the SM scalar potential gets modified which can be seen from Eq (1). In order to ensure that the potential is bounded from below, the quartic couplings in the potential must satisfy the following co-positivity conditions. Following [77, 78] we have derived the copositivity conditions for our present setup:

$$\lambda_H(\mu), \lambda_T(\mu), \lambda_s(\mu) \geq 0 \quad (8a)$$

$$\lambda_{HT}(\mu) + \sqrt{\frac{2}{3}\lambda_H(\mu)\lambda_T(\mu)} \geq 0 \quad (8b)$$

$$\lambda_{HS}(\mu) + \sqrt{\frac{2}{3}\lambda_H(\mu)\lambda_S(\mu)} \geq 0 \quad (8c)$$

$$\kappa(\mu) + \sqrt{\frac{1}{9}\lambda_T(\mu)\lambda_S(\mu)} \geq 0. \quad (8d)$$

where μ is the running scale. These condition should be satisfied at all the energy scales till M_{Pl} in order to ensure the stability of the entire scalar potential in any direction.

- (ii) **Perturbativity:** A perturbative theory expects that the model parameters should obey:

$$|\lambda_i|, |\kappa| < 4\pi \text{ and } |g_i|, |y_{\alpha\beta}| < \sqrt{4\pi}. \quad (9)$$

where λ_i and κ represents the scalar quartic couplings involved in the present setup whereas g_i and $y_{\alpha\beta}$ denotes the SM gauge and Yukawa couplings respectively. We will ensure the perturbativity of the couplings present in the model till the M_{Pl} energy scale by employing the renormalisation group equations (RGE).

- (iii) **Tree level unitarity:** One should also look for the constraints coming from perturbative unitarity associated with the S matrix corresponding to scattering processes involving all two particle initial and final states [79, 80]. In the present setup, there are 13 neutral and 8 singly charged combination of two particle initial/final states. All the details are provided in the Appendix A. The constraints imposed by the tree level

unitarity of the theory are as follows:

$$\begin{aligned}
|\lambda_H| &< 4\pi, \quad \left| \frac{\lambda_T}{3} \right| < 8\pi, \\
|\lambda_{HT}| &< 8\pi, \quad |\lambda_{HS}| < 8\pi, \quad |\kappa| < 8\pi, \\
\text{and } |x_{1,2,3}| &< 16\pi
\end{aligned} \tag{10}$$

where $|x_{1,2,3}|$ are the roots of the following cubic equation:

$$\begin{aligned}
x^3 + x^2(-36\lambda_H - 3\lambda_S - 5\lambda_T) + x(-27\kappa^2 - 36\lambda_{HS}^2 - 108\lambda_{HT}^2 + 108\lambda_H\lambda_S + 180\lambda_H\lambda_T \\
+ 15\lambda_S\lambda_T) + 972\kappa^2\lambda_H - 648\kappa\lambda_{HS}\lambda_{HT} + 324\lambda_{HT}^2 + 180\lambda_{HS}^2\lambda_T\lambda_S - 540\lambda_H\lambda_T\lambda_S \\
= 0.
\end{aligned}$$

B. Experimental constraints

Below we provide a brief discussion of all the important experimental constraints applicable on the present set up.

- (i) **Electroweak precision parameters:** A common approach to study beyond the SM is considering the electroweak precision test. The presence of an additional scalar triplet in the setup may contribute to the oblique parameters. These extra contributions to the oblique parameters coming from the present setup are given as [70, 81, 82]

$$S \simeq 0, \tag{11a}$$

$$T = \frac{1}{8\pi} \frac{1}{s_W^2 c_W^2} \left[\frac{m_{T^0}^2 + m_{T^\pm}^2}{M_Z^2} - \frac{2m_{T^0}^2 m_{T^\pm}^2}{M_Z^2 (m_{T^0}^2 - m_{T^\pm}^2)} \ln \left(\frac{m_{T^0}^2}{m_{T^\pm}^2} \right) \right] \tag{11b}$$

$$\begin{aligned}
&\simeq \frac{1}{6\pi} \frac{1}{s_W^2 c_W^2} \frac{(\Delta m)^2}{M_Z^2} \\
U &= -\frac{1}{3\pi} \left[m_{T^0}^4 \ln \left(\frac{m_{T^0}^2}{m_{T^\pm}^2} \right) \frac{(3m_{T^\pm}^2 - m_{T^0}^2)}{(m_{T^0}^2 - m_{T^\pm}^2)^3} + \frac{5(m_{T^0}^4 + m_{T^\pm}^4) - 22m_{T^0}^2 m_{T^\pm}^2}{6(m_{T^0}^2 - m_{T^\pm}^2)^2} \right] \tag{11c} \\
&\simeq \frac{\Delta m}{3\pi m_{T^\pm}}.
\end{aligned}$$

The contribution to the S parameter from the triplet scalar fields is negligible. It is clear from Eq.(11b) and Eq.(11c) that the contributions to the T and U parameters are also very much suppressed and hence negligible as m_{T^0} and m_{T^\pm} are almost degenerate ($\Delta m = 166$ MeV).

- (ii) **Invisible Higgs decays:** Invisible Higgs decays provide chance for exploring the possible DM-Higgs boson coupling. If the DM particles are lighter than half of the SM Higgs mass (m_h), the Higgs (h) can decay to the DM and can contribute to the invisible Higgs decay. Under such circumstances, we need to employ the bound on the invisible Higgs decay width of the SM Higgs boson as [13]:

$$Br(h \rightarrow \text{Invisible}) < 0.24, \quad (12a)$$

$$\frac{\Gamma(h \rightarrow \text{Invisible})}{\Gamma(h \rightarrow SM) + \Gamma(h \rightarrow \text{Invisible})} < 0.24. \quad (12b)$$

where $\Gamma(h \rightarrow \text{Invisible}) = \Gamma(h \rightarrow T^0 T^0) + \Gamma(h \rightarrow SS)$ when $m_{T^0}, m_S < \frac{m_h}{2}$ and $\Gamma(h \rightarrow SM) = 4.2 \text{ MeV}$. In the present setup we focus mostly in the parameter space where $m_{T^0}, m_S > \frac{m_h}{2}$ so the above constraint is not applicable.

- (iii) **LHC diphoton signal strength:** Due to the presence of the interaction between the SM Higgs h and the triplet scalar T in Eq.(3), the charged triplet scalar T^\pm can contribute significantly to $h \rightarrow \gamma\gamma$ at one loop. The Higgs to diphoton signal strength can be written as

$$\mu_{\gamma\gamma} = \frac{\sigma(gg \rightarrow h \rightarrow \gamma\gamma)_{\text{triplet}}}{\sigma(gg \rightarrow h \rightarrow \gamma\gamma)_{\text{SM}}} \simeq \frac{Br(h \rightarrow \gamma\gamma)_{\text{triplet}}}{Br(h \rightarrow \gamma\gamma)_{\text{SM}}}. \quad (13)$$

$$\frac{Br(h \rightarrow \gamma\gamma)_{\text{triplet}}}{Br(h \rightarrow \gamma\gamma)_{\text{SM}}} = \frac{\Gamma(h \rightarrow \gamma\gamma)_{\text{triplet}}}{\Gamma(h)_{\text{triplet}}} \times \frac{\Gamma(h)_{\text{SM}}}{\Gamma(h \rightarrow \gamma\gamma)_{\text{SM}}}. \quad (14)$$

Now when triplet is heavier than $m_h/2$, we can further write

$$\mu_{\gamma\gamma} = \frac{\Gamma(h \rightarrow \gamma\gamma)_{\text{triplet}}}{\Gamma(h \rightarrow \gamma\gamma)_{\text{SM}}}. \quad (15)$$

The analytic expression of $\Gamma(h \rightarrow \gamma\gamma)_{\text{triplet}}$ can be expressed as [83]

$$\Gamma(h \rightarrow \gamma\gamma) = \frac{G_f \alpha^2 m_h^3}{128 \sqrt{2} \pi^3} \left| \frac{4}{3} \mathcal{A}_{1/2}(x_i) + \mathcal{A}_1(x_i) + 2v \lambda_{HT} \frac{g M_W}{c_W^2 m_{T^\pm}^2} \mathcal{A}_0(x_i) \right|^2. \quad (16)$$

where G_f , is the Fermi constant. The form factors $\mathcal{A}_{1/2}(x_i)$, $\mathcal{A}_1(x_i)$ and $\mathcal{A}_0(x_i)$, are induced by top quark, W gauge boson and T^\pm loop respectively. The formula for the form factors are listed below.

$$\mathcal{A}_{1/2}(x_i) = 2[x_i + (x_i - 1)f(x_i)]x_i^{-2}, \quad (17a)$$

$$\mathcal{A}_1(x_i) = -[3x_i + 2x_i^2 + 3(2x_i - 1)f(x_i)]x_i^{-2}, \quad (17b)$$

$$\mathcal{A}_0(x_i) = -[x_i - f(x_i)]x_i^{-2}. \quad (17c)$$

where $x_i = \frac{m_h^2}{4m_i^2}$ and $f(x) = (\sin^{-1} \sqrt{x})^2$.

In order to ensure that $\mu_{\gamma\gamma}$ lies within the experimental uncertainties, the analysis should respect the latest signal strength from ATLAS [84] and CMS [85]. The measured value of $\mu_{\gamma\gamma}$ are given by $\mu_{\gamma\gamma} = 0.99 \pm 0.14$ from ATLAS and $\mu_{\gamma\gamma} = 1.17 \pm 0.10$ from CMS.

- (iv) **Disappearing charged track:** Despite having an analogous spectrum to the inert Higgs doublet multiplet, the inert Higgs triplet model can not produce similar sort of collider signals as associated with inert Higgs doublet. For example, due to the presence of very small mass splitting among the charged and neutral components, it becomes difficult to look for the collider signals such as di-lepton or multi-leptons plus missing energies in case of inert triplet. Hence, one needs to look for different types of collider signals. The involvement of a charged component (T^\pm) of the triplet scalar in the present scenario provides an interesting discovery prospect at LHC. When produced in pp collisions, the charged triplet scalar can only decays to the neutral component and a soft pion or soft lepton pair (due to the presence of small mass splitting, 166 MeV), after getting produced these soft pions yields a disappearing charged track in the detector. Recently in [72], it was shown that searches for disappearing tracks at LHC presently excludes a real triplet scalar lighter than 287 GeV with $\mathcal{L} = 36 \text{ fb}^{-1}$. The reach can extend to 608 GeV and 761 GeV with the collection of $\mathcal{L} = 300 \text{ fb}^{-1}$ and 3000 fb^{-1} respectively.

- (v) **Relic density and Direct detection of DM:** The parameter space of the present model is to be constrained by the measured value of the DM relic abundance from the Planck experiment [3]. One can further restrict the parameter space by applying bounds on the DM direct detection cross-section coming from the experiments like LUX [4], XENON-1T [5], PandaX-II [6, 7]. Detailed discussions on the dark matter phenomenology are presented in section IV.
- (vi) **LEP constraints:** LEP [86] has set constraints on the masses of the charged and the neutral scalars as $m \geq 100$ GeV from the non-observance of any such related events. We can therefore use the same as a conservative lower bound for the mass of the charged scalar (T^\pm) involved in our construction, $m_{T^\pm} \geq 100$ GeV. In case of scalar triplet, since the mass splitting among the charged and neutral component is of the order of 166 MeV, the same lower bound can be equivalently applied on the mass of the neutral component[87], the DM component.

IV. DARK MATTER PHENOMENOLOGY

The present setup contains two dark matter candidates T^0 and S , both are odd under different discrete symmetries Z_2 and Z'_2 which remain unbroken. To obtain the correct relic densities of the dark matter candidates one needs to solve the coupled Boltzmann equations. In order to do that we first identify all the relevant annihilation channels of both the dark matter candidates. In Fig.1 we show all the possible annihilation channels of S which consists of h mediated s -channels, S mediated t -channel contribution as well as the four point interactions. Similarly in Fig.2, all the relevant annihilation channels for T^0 are indicated. Co-annihilations of T^0 with heavier components of the triplet also contribute to the relic density which are shown in Fig.3. Finally in Fig.4, we show the channels through which one dark matter candidate (heavier one) can be converted to other one (lighter DM). This DM-DM conversion turns out to be an important contribution in obtaining the final relic.

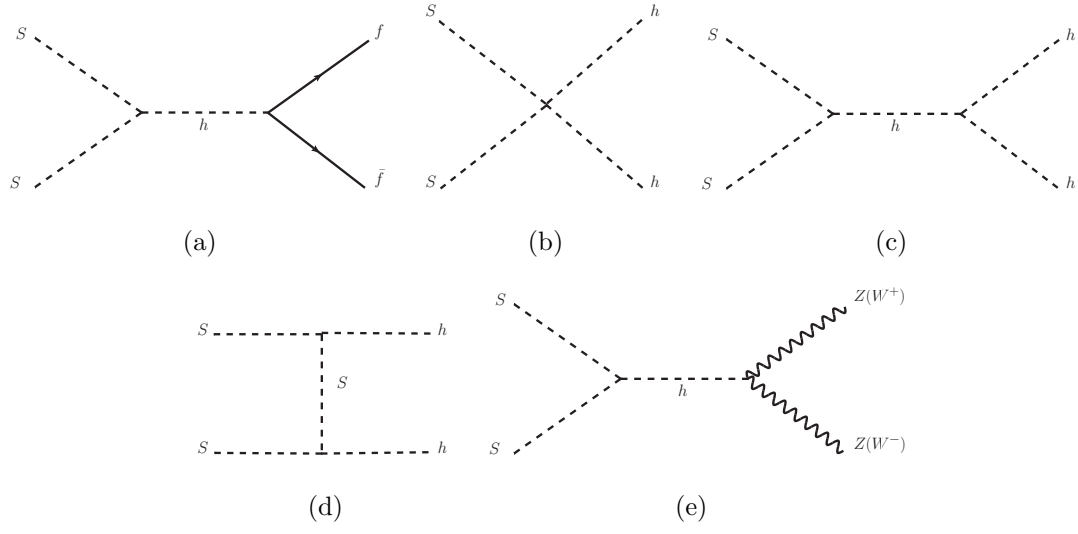


FIG. 1. Annihilation channels for scalar singlet dark matter S .

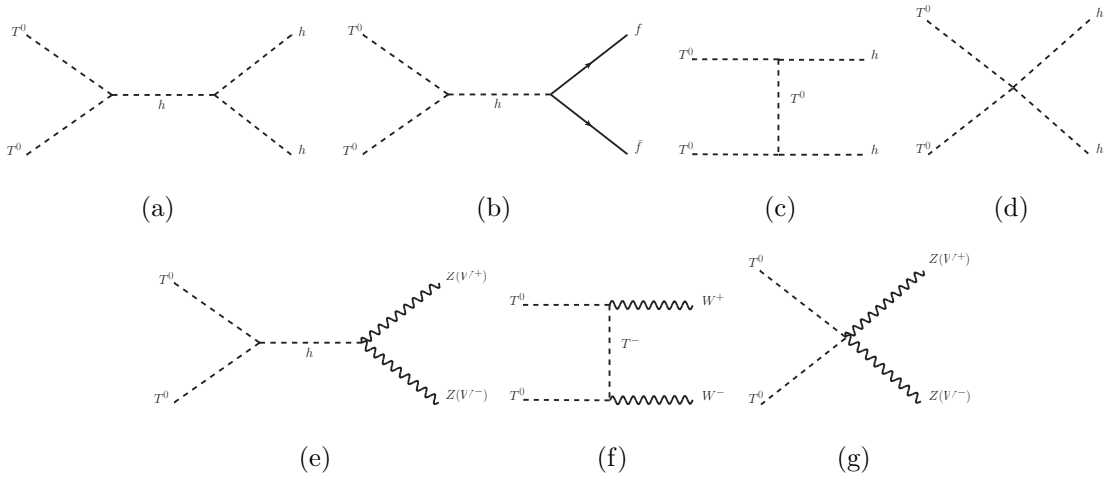


FIG. 2. Annihilation channels for triplet scalar dark matter T^0 .

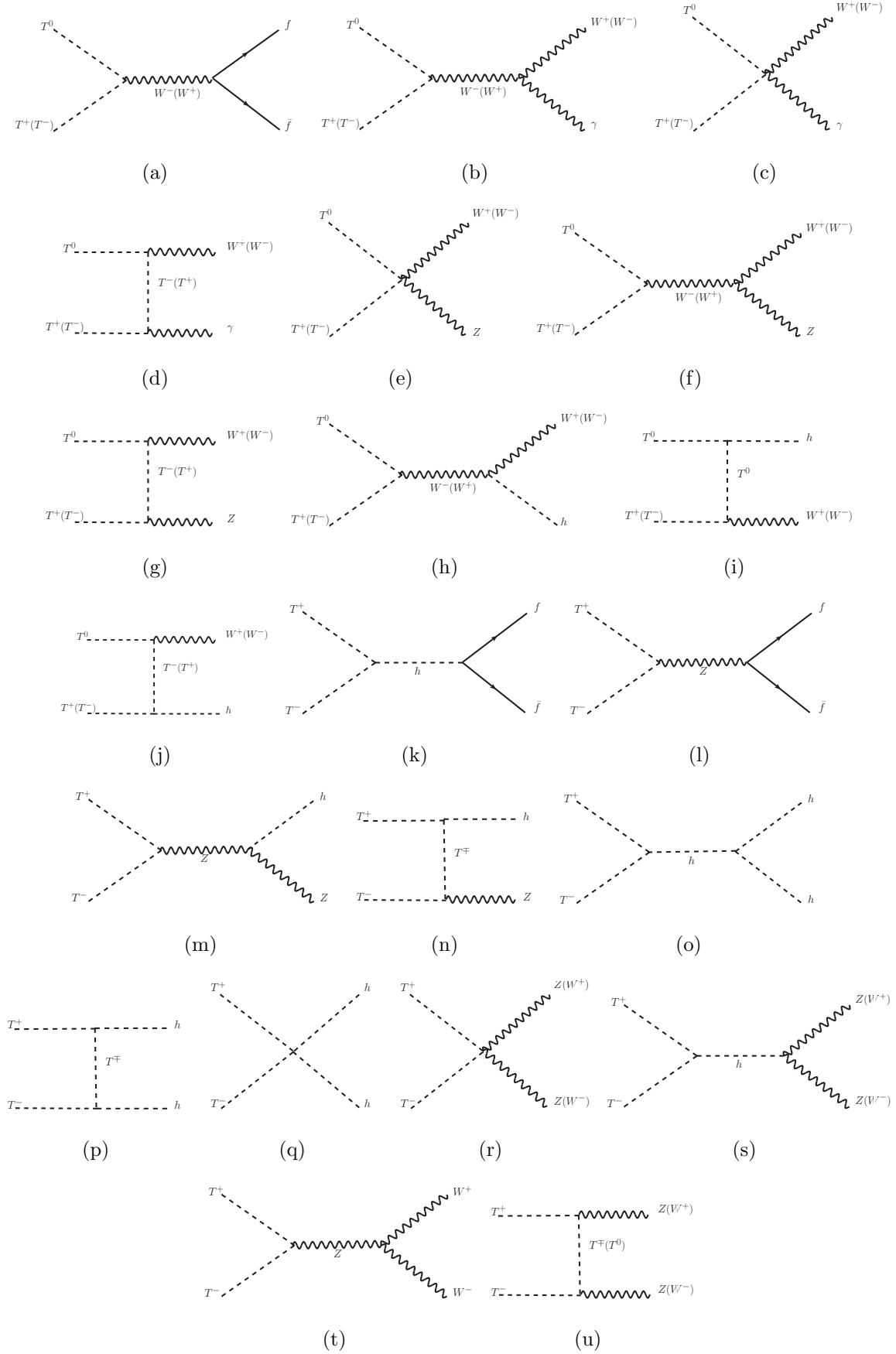


FIG. 3. Co-annihilation (annihilation) channels for triplet scalar dark matter T^0 (T^\pm).

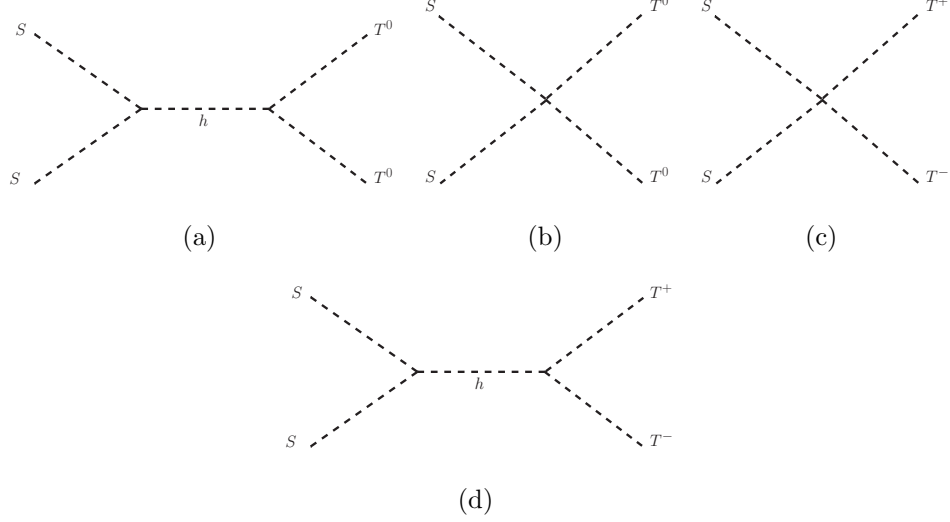


FIG. 4. DM-DM conversion channels between Singlet scalar S and triplet dark matter T^0 , assuming $m_S > m_{T^0}$.

A. Relic Density

To obtain the comoving relic densities corresponding to each dark matter candidates, we need to solve the coupled Boltzmann equations. The involvement of two dark matter candidates leads to the modification in the definition of the x parameter from $\frac{m_{DM}}{T}$ to $\frac{\mu_{dm}}{T}$, where μ_{dm} is the reduced mass expressed as: $\mu_{dm} = \frac{m_S m_{T^0}}{m_S + m_{T^0}}$. One can write the coupled Boltzmann equations, in terms of newly defined parameter $x = \mu_{dm}/T$ and the co-moving number density $Y_{DM} = n_{DM}/s$ (s being the entropy density), as follows¹,

$$\begin{aligned} \frac{dy_S}{dx} = \frac{-1}{x^2} & \left[\langle \sigma v_{SS \rightarrow XX} \rangle \left(y_S^2 - (y_S^{EQ})^2 \right) + \langle \sigma v_{SS \rightarrow T^0 T^0} \rangle \left(y_S^2 - \frac{(y_S^{EQ})^2}{(y_{T^0}^{EQ})^2} y_{T^0}^2 \right) \Theta(m_S - m_{T^0}) \right. \\ & \left. - \langle \sigma v_{T^0 T^0 \rightarrow SS} \rangle \left(y_{T^0}^2 - \frac{(y_{T^0}^{EQ})^2}{(y_S^{EQ})^2} y_S^2 \right) \Theta(m_{T^0} - m_S) \right], \end{aligned} \quad (18a)$$

$$\begin{aligned} \frac{dy_{T^0}}{dx} = \frac{-1}{x^2} & \left[\langle \sigma v_{T^0 T^0 \rightarrow XX} \rangle \left(y_{T^0}^2 - (y_{T^0}^{EQ})^2 \right) + \langle \sigma v_{T^0 T^\pm \rightarrow XX} \rangle \left(y_{T^0} y_{T^\pm} - y_{T^0}^{EQ} y_{T^\pm}^{EQ} \right) + \right. \\ & \langle \sigma v_{T^0 T^0 \rightarrow SS} \rangle \left(y_{T^0}^2 - \frac{(y_{T^0}^{EQ})^2}{(y_S^{EQ})^2} y_S^2 \right) \Theta(m_{T^0} - m_S) - \langle \sigma v_{SS \rightarrow T^0 T^0} \rangle \left(y_S^2 - \frac{(y_S^{EQ})^2}{(y_{T^0}^{EQ})^2} y_{T^0}^2 \right) \\ & \left. \Theta(m_S - m_{T^0}) \right]. \end{aligned} \quad (18b)$$

¹ We use the notation from a recent article on two component DM [28].

Here one can relate y_i ($i = S, T^0$) to Y_i by $y_i = 0.264 M_{Pl} \sqrt{g_*} \mu_{dm} Y_i$ whereas one can redefine $y_i^{EQ} = 0.264 M_{Pl} \sqrt{g_*} \mu_{dm} Y_i^{EQ}$ in terms of equilibrium density Y_i^{EQ} , where the equilibrium distributions (Y_i^{EQ}) are now written in terms of μ_{dm} as

$$Y_i^{EQ}(x) = 0.145 \frac{g}{g_*} x^{3/2} \left(\frac{m_i}{\mu_{dm}} \right)^{3/2} e^{-x \left(\frac{m_i}{\mu_{dm}} \right)}. \quad (19)$$

Here $M_{Pl} = 1.22 \times 10^{19}$ GeV, $g_* = 106.7$, $m_i = m_S, m_{T^0}$, X represents all the SM particles and finally, the thermally averaged annihilation cross-section can be expressed as

$$\langle \sigma v \rangle = \frac{1}{8 m_i^4 T K_2^2 \left(\frac{m_i}{T} \right)} \int_{4m_i^2}^{\infty} \sigma(s - 4m_i^2) \sqrt{s} K_1 \left(\frac{\sqrt{s}}{T} \right) ds \quad (20)$$

and is evaluated at T_f . The freeze-out temperature T_f can be derived by equating the DM interaction rate $\Gamma = n_{DM} \langle \sigma v \rangle$ with the expansion rate of the universe $H(T) \simeq \sqrt{\frac{\pi^2 g_*}{90}} \frac{T^2}{M_{Pl}}$. In Eq.(20), $K_{1,2}(x)$ represents the modified Bessel functions.

We use Θ function in Eq.(18) to explain the conversion process (corresponding to Fig.4) of one dark matter to another which strictly depends on the mass hierarchy of DM particles. These coupled equations can be solved numerically to find the asymptotic abundance of the DM particles, $y_i \left(\frac{\mu_{dm}}{m_i} x_{\infty} \right)$, which can be further used to calculate the relic:

$$\Omega_i h^2 = \frac{854.45 \times 10^{-13}}{\sqrt{g_*}} \frac{m_i}{\mu_{dm}} y_i \left(\frac{\mu_{dm}}{m_i} x_{\infty} \right), \quad (21)$$

where x_{∞} indicates a very large value of x after decoupling. Total DM relic abundance is then given as

$$\Omega_{Total} h^2 = \Omega_{T^0} h^2 + \Omega_S h^2.$$

It is to be noted that total relic abundance must satisfy the DM relic density obtained from Planck [3]

$$\Omega_{Total} h^2 = 0.1199 \pm 0.0027.$$

B. Direct detection

Direct detection (DD) experiments like LUX [4], PandaX-II [6, 7] and Xenon1T [5, 88] look for the indication of the dark matter-nucleon scattering and provide bounds on the

DM-nucleon scattering cross-section. In the present model, dark sector contains two dark matter particles. Therefore, both the dark matter can appear in direct search experiments. However, one should take into account the fact that direct detection of both triplet and singlet DM are to be rescaled by factor f_T^0 (f_S) where $f_j = \frac{\Omega_j}{\Omega_{\text{Total}}}$ with $j = T^0, S$. Therefore, the effective direct detection cross-section of triplet scalar DM T^0 is given as [89]

$$\sigma_{T,\text{eff}} = f_{T^0} \frac{\lambda_{HT}^2}{4\pi} \frac{1}{m_h^4} f^2 \frac{m_N^4}{(m_{T^0} + m_N)^2}, \quad (22)$$

and similarly the effective direct detection cross-section of scalar singlet is expressed as [90]

$$\sigma_{S,\text{eff}} = f_S \frac{\lambda_{HS}^2}{4\pi} \frac{1}{m_h^4} f^2 \frac{m_N^4}{(m_S + m_N)^2}. \quad (23)$$

where m_N is the nucleon mass, λ_{HT} and λ_{HS} are the quartic couplings involved in the DM-Higgs interaction. A recent estimate of the Higgs-nucleon coupling f gives $f = 0.32$ [91]. Below we provide the Feynman diagrams for the spin independent elastic scattering of DM with nucleon.

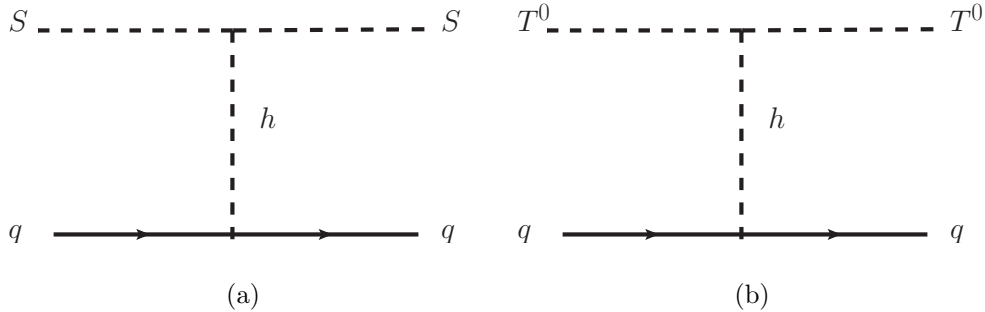


FIG. 5. Spin independent elastic scattering of DM-nucleon.

C. Results

To study the proposed two component DM scenario, we first write the model in LanHEP [76] and then extract the model files to use in micrOMEGAs 4.3.5 [92]. In doing this analysis, all the relevant constraints as mentioned in section III are considered. For the sake of better understanding, we divide our analysis in two parts: [A] $m_S > m_{T^0}$ and [B] $m_{T^0} > m_S$.

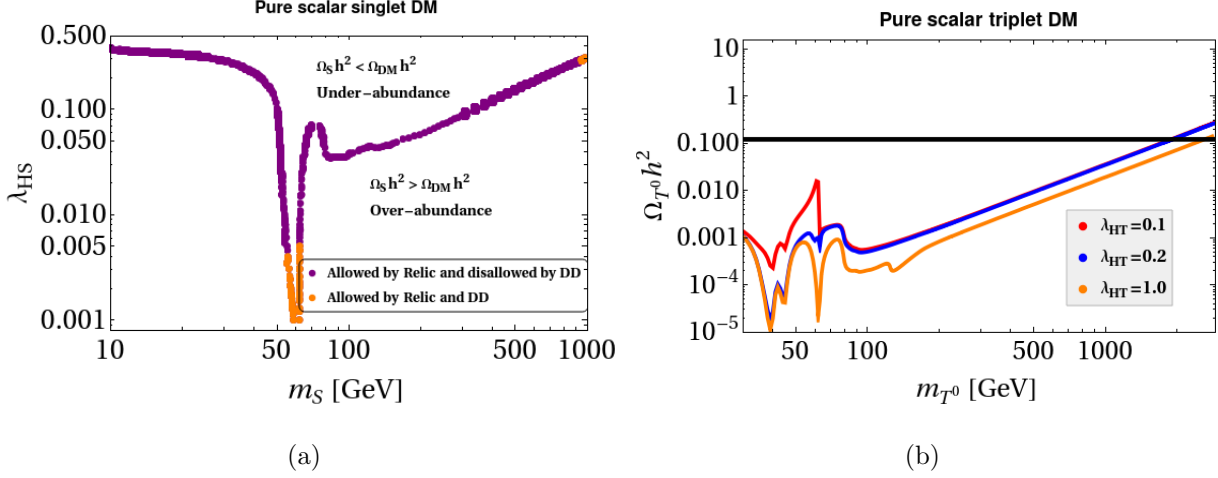


FIG. 6. Single component DM: (a)Left panel: relic contour for singlet scalar DM (b)Right panel: relic contribution from the triplet versus m_{T^0} .

It is known that for a single component DM scenario, both the singlet scalar as well as the triplet (with $Y = 0$) DM are not allowed below TeV. To make it clear, we provide the relic contour for the singlet scalar in the $\lambda_{HS} - m_S$ plane in the left panel of Fig. 6, where except the resonance region, the entire range of m_S up to \sim TeV (the purple shaded region) is ruled out by the DD constraint. Similarly we also include the relic contribution from the triplet against its mass in the right panel of Fig. 6 for different choices of the triplet-SM Higgs portal coupling λ_{HT} . It can clearly be seen that the relic (and DD too) can be satisfied for m_{T^0} beyond 1.8 TeV. Changing the value of λ_{HT} does not have much impact on this conclusion. This is because the effective annihilation cross-section is mostly dominated by the gauge bosons final states contributions, *i.e.*, via Feynman diagrams shown in Fig.2 (annihilations) and Fig.3 (co-annihilations). The presence of first three dips are due to the successive resonances mediated by the W^\pm, Z and SM Higgs (as seen from the s -channel diagrams Fig.3 and Fig.2). The later kinks around 80 GeV and 125 GeV are indicative of the openings of gauge and Higgs boson final states respectively.

Note that our aim is to have mass of both the DM candidates below TeV which is an interesting regime for experimental studies. Here we mostly rely on two facts to satisfy our goal: (i) single component of DM does not require to produce the entire relic contribution and (ii) conversion involving two DMs is expected to contribute non-trivially. Below we proceed one after other cases. As we observe above that the triplet contribution to the relic is essentially under-abundant (irrespective of the choice of portal coupling λ_{HT}) in this

region, we expect that the singlet scalar can make up the rest of relic while an important contribution to be contributed by the DM-DM conversion. As stated before, the relevant parameters that would control the study are m_{T^0} , m_S , λ_{HS} , λ_{HT} , and κ and we find below their importance.

1. Case I: $m_S > m_{T^0}$

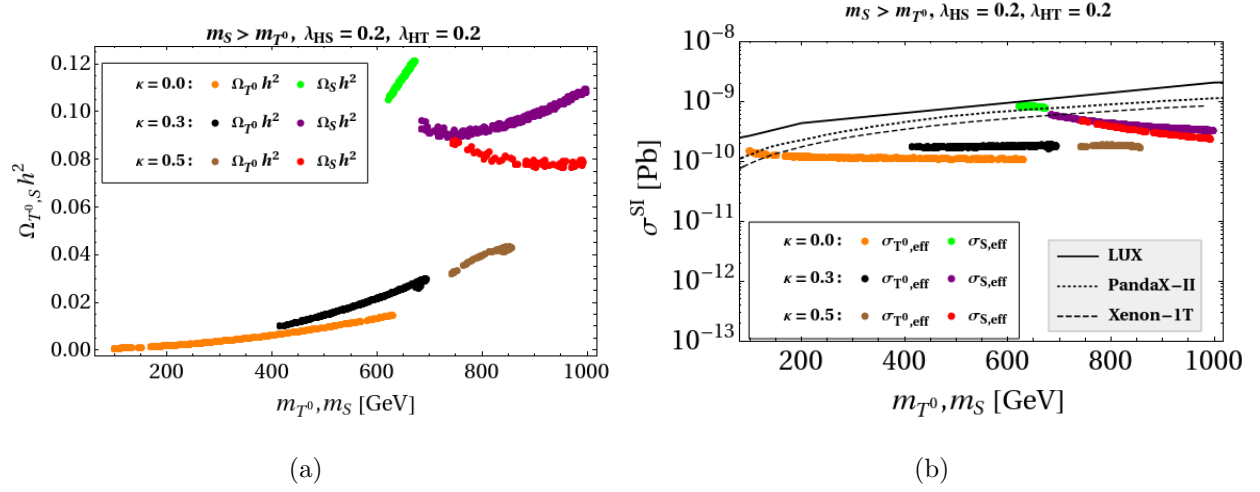


FIG. 7. (a)Left panel: Points which satisfy the correct total DM relic abundance for different values of κ while maintaining $m_S > m_{T^0}$ for $\lambda_{HS} = \lambda_{HT} = 0.2$, (b)Right panel: Spin independent DM-nucleon scattering cross-section. Limits from direct detection experiments are shown in black solid lines (LUX), dotted (PandaX-II), dashed (Xenon-1T).

In the left panel of Fig.7, we show the variation of the individual contributions toward relic abundances from triplet ($\Omega_{T^0} h^2$) and singlet ($\Omega_S h^2$) with their respective masses, m_{T^0} and m_S respectively, such that the total relic abundance $\Omega_{\text{Total}} h^2$ satisfies the Planck limit [3]. In getting such plots, we chose different values of conversion coupling $\kappa = 0, 0.3$ and 0.5 and specifically consider the mass hierarchy as $m_S > m_{T^0}$. The respective variations of the relics versus their masses with different κ are indicated by (i) orange (T^0 contribution) and green (S contribution) patches with $\kappa = 0$, (ii) black (T^0) and purple (S) with $\kappa = 0.3$ and (iii) brown (T^0) and red (S) for $\kappa = 0.5$. Also for simplicity, we choose the Higgs portal couplings (with scalar singlet and triplet) to be same and a reference value is chosen as $\lambda_{HS} = \lambda_{HT} = 0.2$. Note that such a value of the Higgs portal couplings of the singlet and

the triplet scalar DMs is not allowed by the relic and DD constraints as seen from Fig. 6. Below we discuss implications of this plot in detail.

In order to understand the importance of conversion coupling κ , we begin with $\kappa = 0$ case. It is to be noted that even when the conversion coupling κ is set at 0, conversion between DM candidates ($SS \rightarrow T^0 T^0$) can take place via s-channel diagram as shown in Fig. 4. With $\kappa = 0$, we observe that the dominant contribution to the total relic comes from S (the green patch on the top) whereas the contribution coming from T^0 is very small (orange patch near the bottom). To be more precise, a point in the leftmost side of the orange patch (say $m_{T^0} = 100$ GeV having $\Omega_{T^0} h^2 = 0.0005$) is correlated to a single point on the rightmost side of the green patch ($m_S = 667$ GeV with $\Omega_S h^2 = 0.119$). As stated earlier, since triplet annihilation channels are mainly gauge dominated, λ_{HT} does not have a significant effect on the relic density. Hence $\Omega_{T^0} h^2$ has a limitation, it can't provide more than ~ 10 percent contribution as seen from Fig. 6(b). However once the κ has a sizeable magnitude, the T^0 contribution to the relic is enhanced to some extent due to the DM-DM conversion as can be seen from the black patch (paired with purple) for $\kappa = 0.3$ and brown patch (paired with red) for $\kappa = 0.5$. The numerical estimates of several parameters involved in the above discussion are tabulated in Table II for two different choices of the conversion couplings $\kappa = 0.0$ and 0.3 .

κ	m_S [GeV]	m_{T^0} [GeV]	$\Omega_S h^2$	$\Omega_{T^0} h^2$
0.0	667	100	0.119	0.0005
	633	631	0.108	0.014
0.3	999	416	0.108	0.009
	748	695	0.092	0.029

TABLE II. Table showing the variation of the relic densities of both the dark matters with thier respective masses for two different choices of κ . While generating the above results, we considered: $\lambda_{HS} = 0.2$ and $\lambda_{HT} = 0.2$

In Fig. 7(b), the evaluated DD cross-section corresponding to the respective pair of patches of left panel along with the upper limits on DM-nucleon scattering cross-section set by different direct search experiments are depicted. We already notice from the left panel of plots that with $\kappa = 0$, the dominant contribution to the relic comes from S *i.e.* $\frac{\Omega_S}{\Omega_{\text{Total}}} \sim 1$

and hence following Eq. (23), $\sigma_{S,eff}$ is quite large and turns out to be disallowed by the direct detection bounds. This shows that $\kappa = 0$ is not an allowed possibility in this two-component framework. However, as we switch on the DM-DM conversion processes, *i.e.* with $\kappa = 0.3, 0.5$ say, we notice that the intermediate mass range (below TeV) of DMs (which was otherwise disallowed in case of single component scenario for both triplet as well as singlet) becomes allowed from both the relic as well as the direct detection bounds.

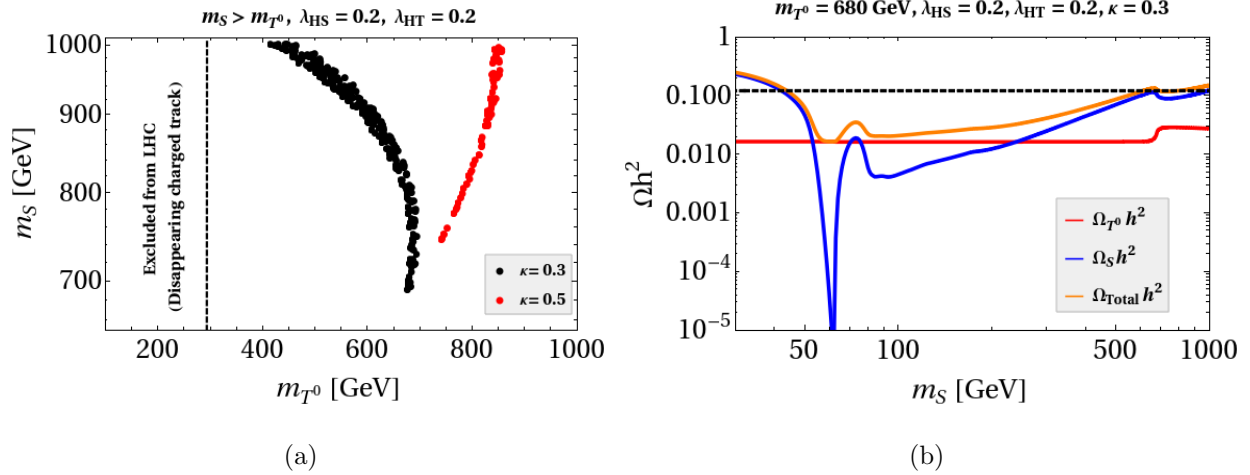


FIG. 8. (a) Left panel shows all the points which satisfy the correct total DM relic abundance and are also allowed by direct detection for different values of κ while maintaining $m_S > m_{T^0}$ for $\lambda_{HS} = 0.2$ and $\lambda_{HT} = 0.2$ in $m_S - m_{T^0}$ plane. (b) Right panel shows the variation of the relic density with m_S for a fixed value $m_{T^0} = 680$ GeV while keeping $\kappa = 0.3$ and $\lambda_{HS} = \lambda_{HT} = 0.2$.

In Fig.8(a), we provide a relic contour plot in $m_S - m_{T^0}$ plane which is also in agreement with bounds from direct detection experiments. It clearly shows that in this two-component scenario allows both the DMs to have mass in the intermediate range or below TeV. It can be noticed that a parabolic pattern is prevalent for the relic contour. The reason of this would be clear if we look at the right panel where individual contributions to the relic ($\Omega_S h^2$ in blue and $\Omega_{T^0} h^2$ in red) are shown as a function of m_S . For this plot (b), the triplet DM mass is kept fixed at 680 GeV while κ is considered to be 0.3 (one of the two benchmark values of Fig. 8(a)). The total relic is shown here by the orange line. We observe that for the singlet scalar contribution, it exactly follows the pattern of its sole contribution (below 680 GeV) as shown in Fig. 6 till it becomes heavier than m_{T^0} . At this point (when $m_{T^0} < m_S$), the $SS \rightarrow T^0 T^0$ starts to take place. As a result, a mild dip is observed on the relic plot of S field around this point and again it increases with the increase of m_S value as usual. On the

other hand, below $m_S = 680$ GeV, there exists a constant contribution (independent of m_S) from T^0 corresponding to fixed mass $m_{T^0} = 680$ GeV as expected. In this case also, when m_S exceeds 680 GeV, we notice an increase in its relic which is reminiscent of the $SS \rightarrow T^0 T^0$ conversion process having $\kappa = 0.3$. The resultant relic plot (orange line) thereby touches the observed relic line ($\Omega_T h^2 = 0.12$) twice: first around $m_S = 690$ GeV and then ~ 801 GeV. The observation that for a fixed m_{T^0} , the total relic would be satisfied by two different values of m_S explains the parabolic nature of black patch in the left panel figure. We also note that for the first pair, the two DM masses [(690, 680) GeV] are very close to each other while within the other pair, DM masses [(801, 680) GeV] are separated by a sizeable value. Once the κ increases, the mass difference between the pair of DM masses (satisfying the relic and DD constraints for a fixed m_{T^0}) would also be increased. For this reason, though the similar observation (satisfaction of relic by two pair of points for a fixed m_{T^0}) is also present for the red patch (with $\kappa = 0.5$), due to the stipulated intermediate regime of DM mass (*i.e.* below TeV) chosen here, the other (the one with heavier m_S) is not seen in the figure.

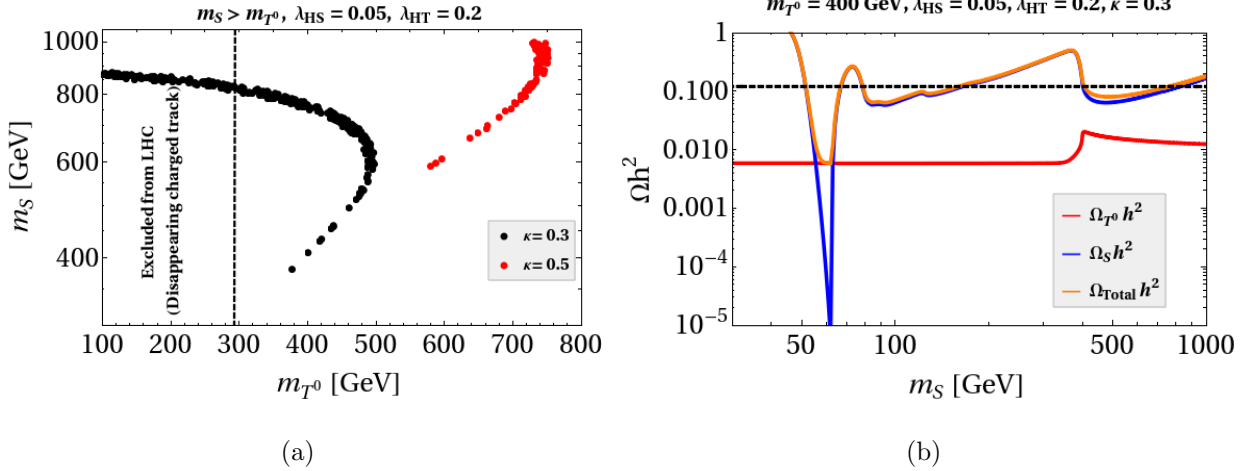


FIG. 9. (a) Points which satisfy the correct total DM relic abundance and are also allowed by direct detection for different values of κ while maintaining $m_S > m_{T^0}$ for $\lambda_{HS} = 0.05$ and $\lambda_{HT} = 0.2$ in $m_S - m_{T^0}$ plane. (b) Variation of Ω_S with m_S for $m_{T^0} = 400$ GeV and $\kappa = 0.3$.

In Fig. 9, we repeat the plots of Fig. 8 for a smaller value of $\lambda_{HS} = 0.05$, though keeping λ_{HT} fixed at 0.2. As λ_{HS} is decreased, the annihilation of S into the SM particles is also decreased which in turn enhances the relic density of S for a given mass. Hence, a relatively smaller contribution from T^0 (compared to Fig. 8(a)) is required and as a result, lower mass

of m_{T^0} is allowed. In other words, a shift of the black patch (of parabolic nature) toward left (*i.e.* shift toward lowered masses) is observed. For example, with the same value of $\kappa = 0.3$ is in Fig. 8 also, while a pair of DM masses $m_S, m_{T^0} = (690, 680)$ GeV satisfies the total relic in case with $\lambda_{HS} = 0.2$, a lower set of masses (407, 400) GeV can satisfy the relic in case with $\lambda_{HS} = 0.05$. At this point, we can recall our finding from Fig. 6 also. The relic contribution from T^0 is essentially governed by the $T^0 T^0$ annihilations to final state gauge bosons, and being almost insensitive to λ_{HT} value, the maximum contribution of $\Omega_{T^0} h^2$ incorporating a sizeable κ can be around 30 percent of the total relic (provided we stick to the low mass regime of DMs, *i.e.* \sim below TeV) with appropriate κ . Therefore the significant relic has to be obtained from S . Hence, the above conclusion that a smaller λ_{HS} allows for a lighter DM pair remains valid for any choice of λ_{HT} . With a similar line of consideration as in Fig. 8(a), here also we use the conservative bound on m_{T^0} as $m_{T^0} > 287$ GeV. Finally in view of constraints on the mass of the triplet DM as stated in section III, we put a vertical dashed line at $m_{T^0} = 287$ GeV such that the right side of it can be recognized as the allowed parameter space. As a result, some of the parameter space becomes disallowed for $\kappa = 0.3$.

2. Case II: $m_S < m_{T^0}$

We now study the DM phenomenology considering the mass hierarchy among DM components as $m_S < m_{T^0}$. Note that in this case the DM-DM conversion can take place having the form: $T^0 T^0 \rightarrow SS$ and hence contribution from the singlet scalar would be more than that of the case-I. Following Fig. 6(b), we know that the maximum contribution of $\Omega_{T^0} h^2$ is less than 30 percent only provided we restrict m_{T^0} to be in sub-TeV regime. Furthermore due to $T^0 T^0 \rightarrow SS$ conversion in this case, contribution to relic by $\Omega_{T^0} h^2$ would be even less. This particular case is therefore not very promising from the perspective of two component DM. Hence in this case, we extend the mass range of T^0 to be more than TeV (though less than 1.8 TeV) while m_S is kept below 1 TeV.

To analyse the case, we scan over the parameter space involving m_S, m_{T^0} with different κ values such that $\Omega_{\text{Total}} h^2$ can satisfy the relic. Here initially the Higgs portal couplings are fixed at values, $\lambda_{HT} = 0.2$ and $\lambda_{HS} = 0.2$ while maintaining the mass hierarchy like $m_S < m_{T^0}$. Though it produces the expected pattern as shown in Fig. 10(a), most of this parameter space are ruled out once DD constraints are applied. There exists only a very

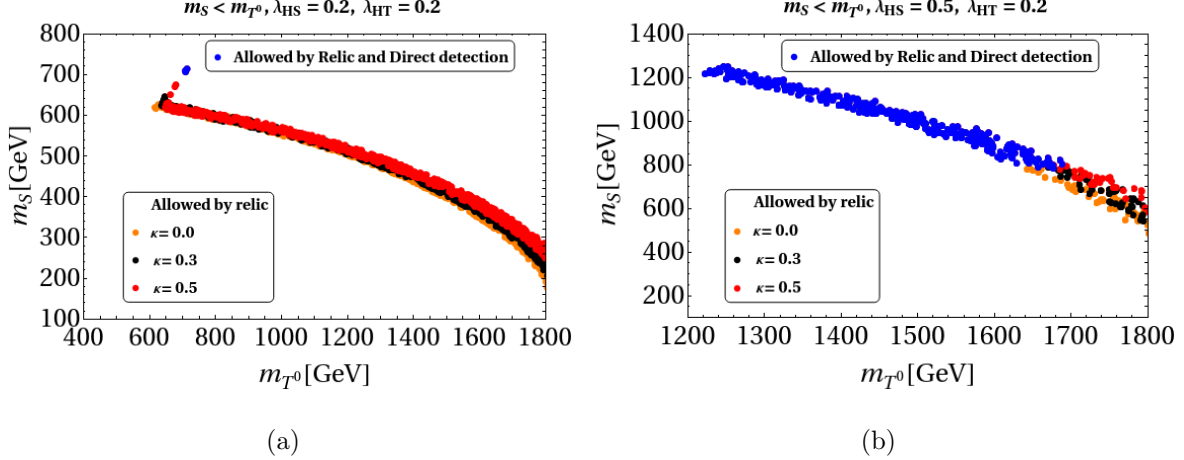


FIG. 10. Points which satisfy the correct total DM relic abundance and are also allowed by direct detection (in blue) for different values of κ while maintaining $m_S < m_{T^0}$ for $\lambda_{HT} = 0.2$ and (a) $\lambda_{HS} = 0.2$ (b) $\lambda_{HS} = 0.5$ in $m_S - m_{T^0}$ plane.

narrow regime corresponding to $\kappa = 0.5$, denoted by the blue shade having masses $m_{T^0} \sim 720$ GeV and $m_S \sim 710$ GeV, which satisfies both the relic and DD limits. Hence it is clear that a large DM-DM conversion is required. However, for the regime where relic satisfied but disallowed by DD, the conversion coupling κ does not have much impact as they (orange points with $\kappa = 0$, black points with $\kappa = 0.3$ and red points with $\kappa = 0.5$) overlap each other. So one can come to a conclusion that this case $m_S < m_{T^0}$ is disfavored compared to the case-I for sub-TeV masses of both the DMs. Also it can be noted that in case-II, due to the parabolic nature of the plot, for a fixed m_{T^0} there are two pairs of values of m_{T^0}, m_S for which relic and DD constraints satisfaction can happen: one is where their masses are close enough and at another point where m_S and m_{T^0} are significantly apart. However such a possibility does not exist here as with a much lower mass of m_S (around 600 GeV) compared to the blue shaded region, the DD constraint is more stringent.

In the right panel, Fig. 10(b), we consider a larger value for $\lambda_{HS} = 0.5$ and simultaneously open the above TeV (but below 1.8 TeV) regime for T^0 DM. Here the relic as well as DD satisfied points are denoted by blue patch and a sizable region of parameter space (compared to the left panel of the figure) becomes allowed and that too for all values of κ . Hence the scenario of two component DM works for a relatively heavier mass, above TeV, of T^0 .

V. ELECTROWEAK VACUUM STABILITY

In this section, we study the electroweak vacuum stability in this two-component DM framework. As already mentioned in section III, Eqs.(8) are to be fulfilled at any scale μ till M_{Pl} . Within SM itself, due to the presence of top quark Yukawa coupling $y_t \sim \mathcal{O}(1)$, the Higgs quartic coupling λ_H becomes negative at a scale around 10^{10} GeV [8–12]. However the present limits on the top quark mass suggests that the EW vacuum is a metastable one. It is well known that incorporating new scalars can modify the fate of the EW vacuum[42–49, 52, 53]. In the present setup, presence of these new scalar fields *i.e.* S and T provides a positive contribution to the beta function of λ_H through their Higgs portal interactions as

$$\beta_{\lambda_H} = \beta_{\lambda_H}^{\text{SM}} + \beta_{\lambda_H}^{\text{T}} + \beta_{\lambda_H}^{\text{S}} = \beta_{\lambda_H}^{\text{SM}} + \frac{3}{2}\lambda_{HT}^2 + \frac{1}{2}\lambda_{HS}^2; \quad (24a)$$

$$\beta_{\lambda_H}^{\text{SM}} = \frac{27}{200}g_1^4 + \frac{9}{20}g_1^2g_2^2 + \frac{9}{8}g_2^4 - \frac{9}{5}g_1^2\lambda_H - 9g_2^2\lambda_H + 24\lambda_H^2 + 12\lambda_H y_t^2 - 6y_t^4. \quad (24b)$$

which (for details, see Appendix B) helps in making the EW vacuum stable.

While $\lambda_H > 0$ till M_{Pl} ensures the absolute stability of the EW vacuum, violation of this at a scale below M_{Pl} could be problematic. In case $\lambda_H(\mu)$ becomes negative at some scale (as happens for SM at Λ_I), there may exist another deeper minimum other than the EW one. Then the estimate of the tunneling probability \mathcal{P}_T of the EW vacuum to the second minimum is essential to confirm the metastability of the Higgs vacuum. The Universe will be in a metastable state, provided the decay time of the EW vacuum is longer than the age of the Universe. The tunneling probability is given by [8, 93],

$$\mathcal{P}_T = T_U^4 \mu_B^4 e^{-\frac{8\pi^2}{3|\lambda_H(\mu_B)|}}, \quad (25)$$

where T_U is the age of the Universe, μ_B is the scale at which the tunneling probability is maximized, determined from $\beta_{\lambda_H}(\mu_B) = 0$. Solving the above equation, the metastability requires:

$$\lambda_H(\mu_B) > \frac{-0.065}{1 - \ln\left(\frac{\nu}{\mu_B}\right)}. \quad (26)$$

At high energies, the RG improved effective potential can be written as [9]

$$V_H^{\text{eff}} = \frac{\lambda_H^{\text{eff}}(\mu)}{4} h^4, \quad (27)$$

where $\lambda_H^{\text{eff}}(\mu) = \lambda_H^{\text{SM,eff}}(\mu) + \lambda_H^{S,\text{eff}}(\mu) + \lambda_H^{T,\text{eff}}(\mu)$. Here, $\lambda_H^{\text{SM,eff}}(\mu)$ is the contribution coming from the SM fields to λ_H whereas $\lambda_H^{S,\text{eff}}(\mu)$ and $\lambda_H^{T,\text{eff}}(\mu)$ are contribution to the λ_H coming from the additional fields S and T in the present setup. These new contributions can be expressed as :

$$\lambda_H^{S,\text{eff}}(\mu) = e^{4\Gamma(h=\mu)} \left[\frac{\lambda_{HS}^2}{64\pi^2} \left(\ln \frac{\lambda_{HS}}{2} - \frac{3}{2} \right) \right] \quad (28a)$$

$$\lambda_H^{T,\text{eff}}(\mu) = e^{4\Gamma(h=\mu)} \left[\frac{3\lambda_{HT}^2}{64\pi^2} \left(\ln \frac{\lambda_{HT}}{2} - \frac{3}{2} \right) \right]. \quad (28b)$$

Here, $\Gamma(h) = \int_{m_t}^h \gamma(\mu) d \ln(\mu)$ and $\gamma(\mu)$ is the anomalous dimension of the Higgs field [8].

In a pure scalar singlet DM scenario, it is known that m_S of the order of TeV is required to make the EW vacuum absolutely stable [34]. On the other hand in a single component hypercharge-less scalar triplet scenario, it is shown that the EW vacuum becomes absolutely stable only if the mass of the scalar triplet particle is around 1.9 TeV. Following the analysis of section IV C with two-component DM scenario made out of S and T^0 , we observe that both the DM can have sub-TeV masses along with relatively smaller values of Higgs portal couplings, λ_{HS} and λ_{HT} . Therefore we would like to explore here whether the same parameter space can make the EW vacuum stable.

Scale	λ_H	y_t	g_1	g_2	g_3
$\mu = m_t$	0.125932	0.93610	0.357606	0.648216	1.16655

TABLE III. Values of the relevant SM couplings (top-quark Yukawa y_t , gauge couplings g_i ($i = 1, 2, 3$) and Higgs quartic coupling λ_H) at energy scale $\mu = m_t = 173.2$ GeV with $m_h = 125.09$ GeV and $\alpha_S(m_Z) = 0.1184$.

For doing the analysis, the running of the SM couplings as well as all the other relevant BSM coupling involved in the present setup is done at two-loops from $\mu = m_t$ to M_{Pl} energy scale² while taking into account the two-loop boundary or matching conditions [95]. In Table III, we provide the initial boundary values (at two-loops) for all SM couplings at an energy scale $\mu = m_t$ in line with [96]. We use these boundary values as evaluated in [8] by taking various threshold corrections at m_t and the mismatch between top pole mass and \overline{MS} renormalized couplings, into account. Here, we consider $m_h = 125.09$ GeV, $m_t = 173.2$

² In Appendix B we only provide the 1-loop β functions which were generated using the model implementation in SARAH [94].

GeV, and $\alpha_S(m_Z) = 0.1184$. A comment on the effect of additional fields (apart from the SM ones) in matching conditions can be pertinent here. In [96], it has been shown that if the Higgs portal coupling(s) of the additional scalar singlet (one DM component here) remains reasonably small ($\mathcal{O}(1)$) while considering mass of the singlet (DM) $\sim \text{TeV}$, the one loop correction observed in the Higgs quartic coupling turns out to be reasonably small in comparison to that of the pure SM. The same conclusion holds for the other DM component as well. As we have considered both the portal couplings as small along with not-so-heavy masses of them, we neglect such corrections in matching conditions while doing the present analysis. Even if those corrections are taken into account, we expect a very mild change in the analysis of vacuum stability.

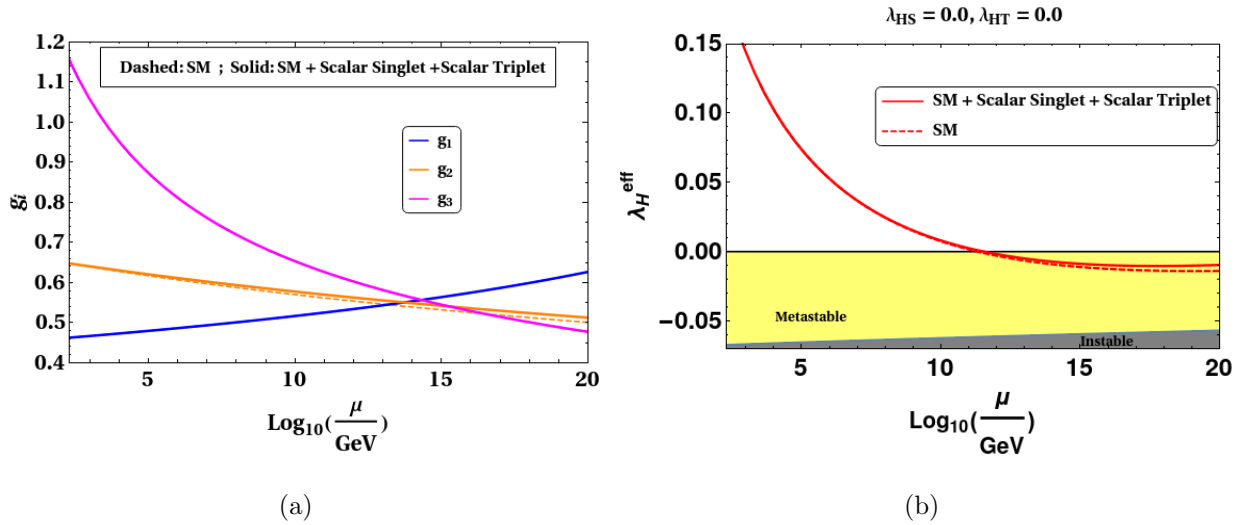


FIG. 11. (a) Left panel compare the evolution of the gauge couplings in the present setup with that of the SM (b) Right panel shows evolution λ_H^{eff} and its comparison with the SM while keeping $\lambda_{HS} = \lambda_{HT} = 0$. In both the panels we have kept $\lambda_{HS} = 0.0$ and $\lambda_{HT} = 0.0$, while keeping $m_{T^0} = 680 \text{ GeV}$, $m_S = 690 \text{ GeV}$ and $\kappa = 0.3$. The colour codings are explained in the legends.

We first show the effect of the scalar triplet on all the gauge couplings g_1, g_2 and g_3 in Fig. 11(a). The newly introduced scalar triplet neither carry a colour charge nor owns hypercharge and hence no modification is observed in the evolution of g_1 (blue) and g_3 (magenta) when compared to the SM ones (solid lines overlaps with the dashed blue and magenta lines). However being charged under $SU(2)$, its inclusion in the present setup increases the number of particles carrying $SU(2)$ charges and hence a modification of the β -function of g_2 is expected via Eq. B(2) in appendix. This positive shift from the SM

BP	m_{T^0} [GeV]	m_S [GeV]	λ_{HS}	λ_{HT}	κ	$\Omega_{T^0} h^2$	$\Omega_S h^2$	$\sigma_{T^0,eff} (pb)$	$\sigma_{S,eff}(pb)$	$\mu_{\gamma\gamma}$
BP-I	680	690	0.2	0.2	0.3	0.026	0.094	1.67×10^{-10}	5.77×10^{-10}	0.998
BP-II	1600	850	0.5	0.2	0.3	0.083	0.034	9.75×10^{-11}	8.84×10^{-10}	0.999

TABLE IV. Benchmark points for which the total relic density satisfy the Planck limit and are also allowed by the direct detection experiments. The following BPs are also allowed by the constraints coming from ATLAS on the Higgs signal strength $\mu_{\gamma\gamma}$.

values (dashed orange line) is also depicted in the running of g_2 (orange line) in Fig. 11(a). The increase in the value of g_2 at high scales also impacts the evolution of effective Higgs quartic coupling λ_H^{eff} to some extent which can be seen from the Fig. 11(b) where all the Higgs portal couplings are set to zero. This positive shift in λ_H^{eff} is observed due to the presence of term proportional to g_2^4 in Eq. (24 b). Even though a positive shift is observed in the evolution of λ_H^{eff} in Fig. 11(b), it is very moderate and hence fails to make the EW vacuum absolutely stable. The absolute stability of the EW vacuum can be obtained once the Higgs portal couplings are switched on.

As stated above, both the couplings λ_{HS} and λ_{HT} (with different pre-factors) play a significant role in the running of effective Higgs quartic coupling λ_H^{eff} . Presence of these Higgs portal couplings are therefore expected to make the EW vacuum stable. For the analysis purpose, we have chosen two benchmark points BP-I and BP-II as shown in Table IV. Both these points satisfy the total relic density, the direct detection bounds and are also allowed by the constraints coming from ATLAS [84] on the Higgs signal strength $\mu_{\gamma\gamma}$ (as discussed in section III). While choosing the benchmark points we have kept κ fixed at 0.3 so that the conversion of the heavier dark matter to the lighter one remains effective. We here fix the scalar singlet DM mass $m_S = 690$ GeV for BP-I and 850 GeV for BP-II along with the choices of $\lambda_{HS} = 0.2$ (BP-I) and 0.5 (BP-II) respectively. Note that such choices of m_S and λ_{HS} neither allow S to be a single component DM nor they make the effective Higgs quartic coupling λ_H^{eff} positive all the way till M_{Pl} .

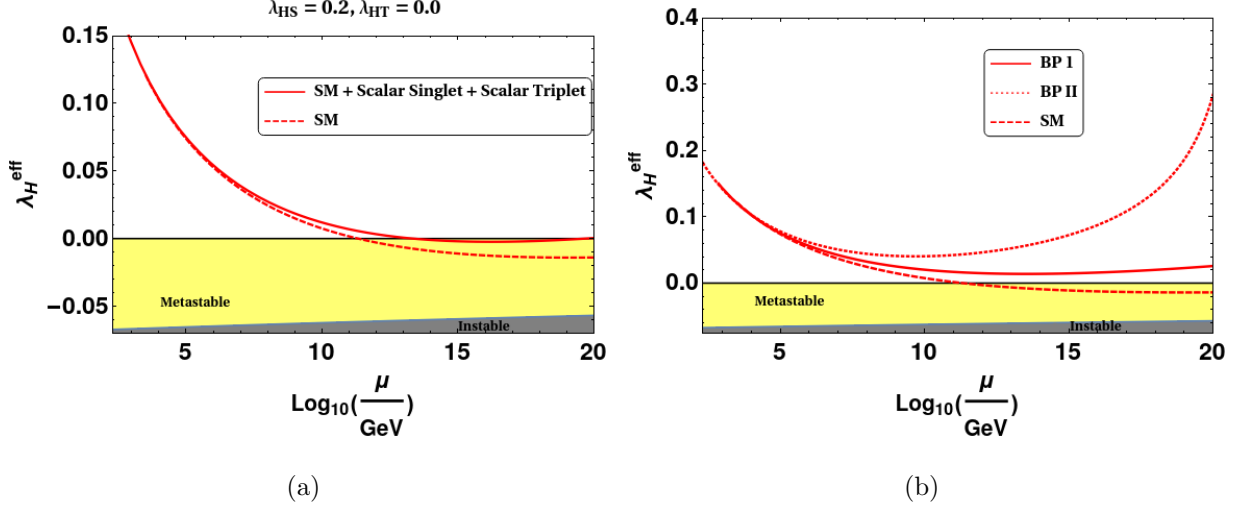


FIG. 12. Evolution of effective Higgs quartic coupling λ_H^{eff} against the scale μ for (a) $\lambda_{HS} = 0.2$ and $\lambda_{HT} = 0.0$, while keeping $m_{T^0} = 680$ GeV, $m_S = 690$ GeV and $\kappa = 0.3$ (b) two given benchmark points BP-I (solid red lines) and BP-II (dotted red lines).

In Fig. 12 (a) we first show the effect of the Higgs portal coupling λ_{HS} on the running of λ_H^{eff} while keeping $\lambda_{HT} = 0$. As discussed above, once the Higgs portal coupling λ_{HS} is switched on, it tends to push the λ_H^{eff} towards the larger value. At this moment, one may recall that $\lambda_{HS} = 0.3$ or above is required to make the EW vacuum absolutely stable just by introducing the singlet scalar S [51]. Here we will see that with $\lambda_{HS} \leq 0.2$, the EW vacuum can be absolutely stable, thanks to the other Higgs portal coupling λ_{HT} . In Fig. 12 (b) we show the running of the effective Higgs quartic coupling λ_H^{eff} in our model for the two benchmark points as mentioned in Table IV, BP-I (solid red lines) as well as BP-II (dotted red lines) and compare it with that of the SM (dashed red lines). As expected, we observe in Fig. 12(b) that due to the presence of both scalar couplings λ_{HS} and λ_{HT} , the β_{λ_H} gets affected and hence make λ_H^{eff} positive till M_{Pl} . The conclusion remains valid for both the benchmark points, BP-I and BP-II. Increase in the value of λ_H^{eff} for BP-II is due of the involvement of larger $\lambda_{HS} = 0.5$.

In Fig. 13, we plot the running of all the scalar quartic couplings in our model for both the BPs. We observe in Fig. 13 that all the couplings remain positive and perturbative till the Planck scale M_{Pl} for both the BPs. Here we have used the central values of top mass and α_s . It can be noted that if we allow a 3σ variation of m_t and m_s , there would be some positive shift in the running of λ_H^{eff} even within the pure SM case corresponding

to the smallest value of top mass and the largest value of α_s (in their 3σ allowed range). However we have found that that such a shift cannot be comparable to the ones obtained in our scenario for BP-I and II. It is also interesting to note that the self quartic coupling of the scalar singlet S in Fig. 13 (b) shoots up, this happens because of the specific choice of $\lambda_{HS} = 0.5$ made in BP-II as shown in Table IV. This rapid increase in the evolution of λ_S for the large value of λ_{HS} is dictated by the presence of $12\lambda_{HS}^2$ term in the β_{λ_S} .

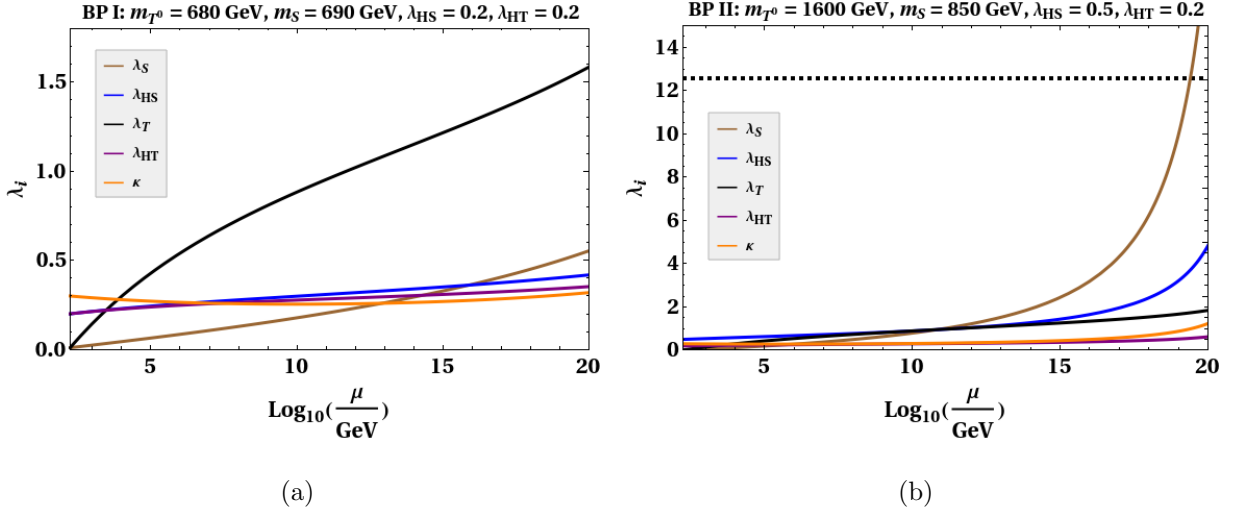


FIG. 13. (a) Left panel shows evolution of the quartic couplings involved in the present setup for BP-I (b) Right panel shows evolution of the same quartic couplings for BP-II. The colour codings are explained in the legends.

VI. CONCLUSIONS

In this work, we explore a two-component DM scenario made out of one singlet scalar and the neutral component of a hypercharge-less triplet scalar. As a single component dark matter, none of these candidates satisfies the relic density and the DD constraints having mass below TeV. While the singlet scalar starts to satisfy the relic and DD with its mass close to 1 TeV alone, the $Y = 0$ triplet can do so with its mass close to 2 TeV. Hence we particularly focus in this sub-TeV region as this regime is otherwise an interesting one from the perspective of collider and dark matter experiments. We are able to show that the DM-DM conversions becomes helpful so as to realize our goal of restricting both the dark matters in sub-TeV regime for $m_S > m_{T^0}$. In case of reverse mass hierarchy, such a realization turns out to be not that favorable though. In this case where $m_S < m_{T^0}$, triplet

mass beyond 1 TeV (but much less than 2 TeV) with m_S below 1 TeV can do the job.

In this entire analysis, the conversion coupling κ plays a pivotal role. We observe that though it is mostly the scalar singlet contribution which contributes dominantly to the relic, the parameter space with $\kappa = 0$ is completely disallowed. This is due to the fact that the relic density then would be mainly followed from S only and hence the effective cross-section in DD can not have adequate suppression which is otherwise expected via Eq.(23) with a sizeable κ . The parameter space that satisfy the relic and DD constraints is also consistent in making the electroweak vacuum absolutely stable. This is mainly achieved through the contributions of the Higgs portal couplings of the dark matters. The setup also bears an interesting discovery potential at LHC. Due to its multi-component nature, the present setup can accommodate smaller value of triplet scalar mass (below TeV) which provides a possibility of probing the charged scalar more proficiently at LHC via the disappearing charge track at the detector. A detailed study in this direction remain an interesting possibility to explore in future.

ACKNOWLEDGMENTS

A.D.B and A.S acknowledge the support from DST, Government of India, under Grant No. PDF/2016/002148 during the early phase of the work where A.D.B was supported by the SERB National Post-Doctoral fellowship under the same. A.D.B is also supported by the National Science Foundation of China (11422545,11947235). RR would like to thank Najimuddin Khan for various useful discussions during the course of this work.

Appendix A: Tree level unitarity constraints

In this section we discuss the perturbative unitarity limits on the quartic coupling present in our model. The scattering amplitude for any $2 \rightarrow 2$ process can be expressed in terms of the Legendre polynomial as [97]

$$\mathcal{M}^{2 \rightarrow 2} = 16\pi \sum_{l=0}^{\infty} a_l (2l+1) P_l(\cos \theta) \quad (\text{A1})$$

where θ is the scattering angle and $P_l(\cos \theta)$ is the Legendre polynomial of order l . In the high energy limit, only the s-wave ($l = 0$) partial amplitude a_0 will determine the leading

energy dependence of the scattering process. The unitarity constraint says

$$\text{Re } |a_0| < \frac{1}{2} \quad (\text{A2})$$

This constraint in Eq.(A2) can be further converted to a bound on the scattering amplitude \mathcal{M}

$$|\mathcal{M}| < 8\pi \quad (\text{A3})$$

In our present setup, we have multiple possible $2 \rightarrow 2$ scattering process. Therefore, we need to construct a matrix ($\mathcal{M}_{i,j}^{2 \rightarrow 2} = \mathcal{M}_{i \rightarrow j}$) considering all the two particle states. Finally we need to calculate the eigenvalues of \mathcal{M} and employ the bound as in Eq. (A3). In the high-energy limit, we express the SM Higgs doublet as $H^T = (w^+ \frac{h+iz}{\sqrt{2}})$. Then the scalar potential in Eq.(p1) give rise to 13 neutral combinations of two particle states:

$$w^+w^-, \frac{hh}{\sqrt{2}}, \frac{zz}{\sqrt{2}}, T^+T^-, \frac{T^0T^0}{\sqrt{2}}, \frac{SS}{\sqrt{2}}, hT^0, zT^0, hS, zS, hz, w^+T^-, T^+w^- \quad (\text{A4})$$

and 8 singly charged two particle states:

$$w^+h, w^+z, w^+T^0, w^+S, T^+T^0, T^+h, T^+z, T^+S. \quad (\text{A5})$$

Therefore, we can write the scattering amplitude matrix (M) in block diagonal form by decomposing it into a neutral (NS) and singly charged (CS) sector as

$$M_{21 \times 21} = \begin{pmatrix} (M^{NS})_{13 \times 13} & 0 \\ 0 & (M^{CS})_{8 \times 8} \end{pmatrix}. \quad (\text{A6})$$

where the submatrices are given by

$$M_{13 \times 13}^{NS} = \begin{pmatrix} (M_1^{NS})_{6 \times 6} & 0 \\ 0 & (M_2^{NS})_{7 \times 7} \end{pmatrix}. \quad (\text{A7})$$

with

$$M_1^{NS} = \begin{pmatrix} 4\lambda_H & \sqrt{2}\lambda_H & \sqrt{2}\lambda_H & \lambda_{HT} & \frac{\lambda_{HT}}{\sqrt{2}} & \frac{\lambda_{HS}}{\sqrt{2}} \\ \sqrt{2}\lambda_H & 3\lambda_H & \lambda_H & \frac{\lambda_{HT}}{\sqrt{2}} & \frac{\lambda_{HT}}{2} & \frac{\lambda_{HS}}{2} \\ \sqrt{2}\lambda_H & \lambda_H & 3\lambda_H & \frac{\lambda_{HT}}{\sqrt{2}} & \frac{\lambda_{HT}}{2} & \frac{\lambda_{HS}}{2} \\ \lambda_{HT} & \frac{\lambda_{HT}}{\sqrt{2}} & \frac{\lambda_{HT}}{\sqrt{2}} & \frac{2\lambda_T}{3} & \frac{\lambda_T}{3\sqrt{2}} & \frac{\kappa}{\sqrt{2}} \\ \frac{\lambda_{HT}}{\sqrt{2}} & \frac{\lambda_{HT}}{2} & \frac{\lambda_{HT}}{2} & \frac{\lambda_T}{3\sqrt{2}} & \frac{\lambda_T}{2} & \frac{\kappa}{2} \\ \frac{\lambda_{HS}}{\sqrt{2}} & \frac{\lambda_{HS}}{2} & \frac{\lambda_{HS}}{2} & \frac{\kappa}{\sqrt{2}} & \frac{\kappa}{2} & \frac{\lambda_S}{2} \end{pmatrix}, \quad (\text{A8})$$

$$M_2^{NS} = \begin{pmatrix} \lambda_{HT} & 0 & 0 & 0 & 0 & 0 & 0 \\ 0 & \lambda_{HT} & 0 & 0 & 0 & 0 & 0 \\ 0 & 0 & \lambda_{HS} & 0 & 0 & 0 & 0 \\ 0 & 0 & 0 & \lambda_{HS} & 0 & 0 & 0 \\ 0 & 0 & 0 & 0 & 2\lambda_H & 0 & 0 \\ 0 & 0 & 0 & 0 & 0 & \lambda_{HT} & 0 \\ 0 & 0 & 0 & 0 & 0 & 0 & \lambda_{HT} \end{pmatrix}, \quad (\text{A9})$$

and

$$M^{CS} = \begin{pmatrix} 2\lambda_H & 0 & 0 & 0 & 0 & 0 & 0 & 0 \\ 0 & 2\lambda_H & 0 & 0 & 0 & 0 & 0 & 0 \\ 0 & 0 & \lambda_{HT} & 0 & 0 & 0 & 0 & 0 \\ 0 & 0 & 0 & \lambda_{HS} & 0 & 0 & 0 & 0 \\ 0 & 0 & 0 & 0 & \frac{\lambda_T}{3} & 0 & 0 & 0 \\ 0 & 0 & 0 & 0 & 0 & \lambda_{HT} & 0 & 0 \\ 0 & 0 & 0 & 0 & 0 & 0 & \lambda_{HT} & 0 \\ 0 & 0 & 0 & 0 & 0 & 0 & 0 & \kappa \end{pmatrix}. \quad (\text{A10})$$

After determining the eigenvalues of Eq.(A6) we conclude that the tree level unitarity constraints in this setup are the following:

$$\begin{aligned} |\lambda_H| &< 4\pi, \quad \left| \frac{\lambda_T}{3} \right| < 8\pi, \\ |\lambda_{HT}| &< 8\pi, \quad |\lambda_{HS}| < 8\pi, \quad |\kappa| < 8\pi, \\ \text{and } |x_{1,2,3}| &< 16\pi \end{aligned} \quad (\text{A11})$$

where $|x_{1,2,3}|$ are the roots of the following cubic equation:

$$\begin{aligned}
& x^3 + x^2(-36\lambda_H - 3\lambda_S - 5\lambda_T) + x(-27\kappa^2 - 36\lambda_{HS}^2 - 108\lambda_{HT}^2 + 108\lambda_H\lambda_S + 180\lambda_H\lambda_T \\
& + 15\lambda_S\lambda_T) + 972\kappa^2\lambda_H - 648\kappa\lambda_{HS}\lambda_{HT} + 324\lambda_{HT}^2 + 180\lambda_{HS}^2\lambda_T\lambda_S - 540\lambda_H\lambda_T\lambda_S \\
& = 0.
\end{aligned}$$

Appendix B: 1-loop β -functions

Below we provide the 1-loop β -functions for all the couplings involved in the present setup. While generating the β -functions we have considered one scalar singlet and one hyperchargeless scalar triplet together with the SM particle spectrum. Since the new particles do not carry any colour charges and the Yukawa interactions of these particles are forbidden due to the symmetry assignment of the setup, no modification is observed in the β -function of the strong coupling g_3 and the top Yukawa coupling y_t . The hypercharge being zero for both the BSM fields, the β -function of gauge coupling g_1 remain same as that of the $\beta_{g_1}^{\text{SM}}$ whereas T being a $SU(2)$ triplet, a shift in the β -function of g_2 can be observed in comparison to that of the $\beta_{g_2}^{\text{SM}}$.

a. SM Couplings

$$\beta_{g_1} = \beta_{g_1}^{\text{SM}} + \beta_{g_1}^{\text{T}} + \beta_{g_1}^{\text{S}} = \beta_{g_1}^{\text{SM}} \quad (\text{B1})$$

$$\beta_{g_2} = \beta_{g_2}^{\text{SM}} + \beta_{g_2}^{\text{T}} + \beta_{g_2}^{\text{S}} = \beta_{g_2}^{\text{SM}} + \frac{g_2^3}{16\pi^2} \left(\frac{1}{3} \right) \quad (\text{B2})$$

$$\beta_{g_3} = \beta_{g_3}^{\text{SM}} + \beta_{g_3}^{\text{T}} + \beta_{g_3}^{\text{S}} = \beta_{g_3}^{\text{SM}} \quad (\text{B3})$$

$$\beta_{\lambda_H} = \beta_{\lambda_H}^{\text{SM}} + \beta_{\lambda_H}^{\text{T}} + \beta_{\lambda_H}^{\text{S}} = \beta_{\lambda_H}^{\text{SM}} + \frac{3}{2}\lambda_{HT}^2 + \frac{1}{2}\lambda_{HS}^2 \quad (\text{B4})$$

$$\beta_{y_t} = \beta_{y_t}^{\text{SM}} + \beta_{y_t}^{\text{T}} + \beta_{y_t}^{\text{S}} = \beta_{y_t}^{\text{SM}} \quad (\text{B5})$$

b. BSM couplings

$$\beta_{\lambda_S} = 3(3\kappa^2 + 4\lambda_{HS}^2 + \lambda_S^2) \quad (\text{B6})$$

$$\beta_{\lambda_{HS}} = 3\kappa\lambda_{HT} - \frac{9}{10}g_1^2\lambda_{HS} - \frac{9}{2}g_2^2\lambda_{HS} + 12\lambda_H\lambda_{HS} + \lambda_S\lambda_{HS} + 4\lambda_{HS}^2 + 6\lambda_{HS}y_t^2 \quad (\text{B7})$$

$$\beta_{\lambda_T} = 12\lambda_{HT}^2 - 24g_2^2\lambda_T + 3\kappa^2 + 72g_2^4 + \frac{11}{3}\lambda_T^2 \quad (\text{B8})$$

$$\beta_{\lambda_{HT}} = 6g_2^4 - \frac{9}{10}g_1^2\lambda_{HT} - \frac{33}{2}g_2^2\lambda_{HT} + 12\lambda_H\lambda_{HT} + 4\lambda_{HT}^2 + \kappa\lambda_{HS} + \frac{5}{3}\lambda_{HT}\lambda_T + 6\lambda_{HT}y_t^2 \quad (\text{B9})$$

$$\beta_{\kappa} = -12g_2^2\kappa + 4\kappa^2 + 4\lambda_{HT}\lambda_{HS} + \kappa\left(\frac{5}{3}\lambda_T + \lambda_S\right) \quad (\text{B10})$$

-
- [1] S. Chatrchyan et al. (CMS), Phys. Lett. **B716**, 30 (2012), 1207.7235.
 - [2] G. Aad et al. (ATLAS), Phys. Lett. **B716**, 1 (2012), 1207.7214.
 - [3] N. Aghanim et al. (Planck) (2018), 1807.06209.
 - [4] D. S. Akerib et al. (LUX), Phys. Rev. Lett. **118**, 021303 (2017), 1608.07648.
 - [5] E. Aprile et al. (XENON), Phys. Rev. Lett. **121**, 111302 (2018), 1805.12562.
 - [6] A. Tan et al. (PandaX-II), Phys. Rev. Lett. **117**, 121303 (2016), 1607.07400.
 - [7] X. Cui et al. (PandaX-II), Phys. Rev. Lett. **119**, 181302 (2017), 1708.06917.
 - [8] D. Buttazzo, G. Degrandi, P. P. Giardino, G. F. Giudice, F. Sala, A. Salvio, and A. Strumia, JHEP **12**, 089 (2013), 1307.3536.
 - [9] G. Degrandi, S. Di Vita, J. Elias-Miro, J. R. Espinosa, G. F. Giudice, G. Isidori, and A. Strumia, JHEP **08**, 098 (2012), 1205.6497.
 - [10] Y. Tang, Mod. Phys. Lett. **A28**, 1330002 (2013), 1301.5812.
 - [11] J. Ellis, J. R. Espinosa, G. F. Giudice, A. Hoecker, and A. Riotto, Phys. Lett. **B679**, 369 (2009), 0906.0954.
 - [12] J. Elias-Miro, J. R. Espinosa, G. F. Giudice, G. Isidori, A. Riotto, and A. Strumia, Phys. Lett. **B709**, 222 (2012), 1112.3022.
 - [13] M. Tanabashi et al. (Particle Data Group), Phys. Rev. **D98**, 030001 (2018).

- [14] A. Biswas, D. Majumdar, A. Sil, and P. Bhattacharjee, JCAP **1312**, 049 (2013), 1301.3668.
- [15] O. Fischer and J. J. van der Bij, Mod. Phys. Lett. **A26**, 2039 (2011).
- [16] S. Bhattacharya, A. Drozd, B. Grzadkowski, and J. Wudka, JHEP **10**, 158 (2013), 1309.2986.
- [17] L. Bian, R. Ding, and B. Zhu, Phys. Lett. **B728**, 105 (2014), 1308.3851.
- [18] S. Esch, M. Klasen, and C. E. Yaguna, JHEP **09**, 108 (2014), 1406.0617.
- [19] A. Karam and K. Tamvakis, Phys. Rev. D **92**, 075010 (2015), 1508.03031.
- [20] A. Karam and K. Tamvakis, Phys. Rev. D **94**, 055004 (2016), 1607.01001.
- [21] S. Bhattacharya, P. Poulose, and P. Ghosh, JCAP **1704**, 043 (2017), 1607.08461.
- [22] A. Dutta Banik, M. Pandey, D. Majumdar, and A. Biswas, Eur. Phys. J. C **77**, 657 (2017), 1612.08621.
- [23] A. Ahmed, M. Duch, B. Grzadkowski, and M. Iglicki, Eur. Phys. J. **C78**, 905 (2018), 1710.01853.
- [24] J. Herrero-Garcia, A. Scaffidi, M. White, and A. G. Williams, JCAP **1711**, 021 (2017), 1709.01945.
- [25] J. Herrero-Garcia, A. Scaffidi, M. White, and A. G. Williams, JCAP **1901**, 008 (2019), 1809.06881.
- [26] A. Poulin and S. Godfrey, Phys. Rev. **D99**, 076008 (2019), 1808.04901.
- [27] M. Aoki and T. Toma, JCAP **1810**, 020 (2018), 1806.09154.
- [28] S. Bhattacharya, P. Ghosh, and N. Sahu, JHEP **02**, 059 (2019), 1809.07474.
- [29] M. Aoki, D. Kaneko, and J. Kubo, Front.in Phys. **5**, 53 (2017), 1711.03765.
- [30] B. Barman, S. Bhattacharya, and M. Zakeri, JCAP **1809**, 023 (2018), 1806.01129.
- [31] S. Chakraborti, A. Dutta Banik, and R. Islam, Eur. Phys. J. C **79**, 662 (2019), 1810.05595.
- [32] F. Elahi and S. Khatibi, Phys. Rev. **D100**, 015019 (2019), 1902.04384.
- [33] D. Borah, R. Roshan, and A. Sil (2019), 1904.04837.
- [34] S. Bhattacharya, P. Ghosh, A. K. Saha, and A. Sil (2019), 1905.12583.
- [35] A. Biswas, D. Borah, and D. Nanda (2019), 1908.04308.
- [36] S. Bhattacharya, N. Chakraborty, R. Roshan, and A. Sil (2019), 1910.00612.
- [37] D. Nanda and D. Borah (2019), 1911.04703.
- [38] T. N. Maity and T. S. Ray, Phys. Rev. D **101**, 103013 (2020), 1908.10343.
- [39] S. Khalil, S. Moretti, D. Rojas-Ciofalo, and H. Waltari (2020), 2007.10966.
- [40] G. Bélanger, A. Pukhov, C. E. Yaguna, and A. Zapata (2020), 2006.14922.

- [41] C. H. Nam, D. Van Loi, L. X. Thuy, and P. Van Dong (2020), 2006.00845.
- [42] N. Haba, K. Kaneta, and R. Takahashi, JHEP **04**, 029 (2014), 1312.2089.
- [43] N. Khan and S. Rakshit, Phys. Rev. **D90**, 113008 (2014), 1407.6015.
- [44] V. V. Khoze, C. McCabe, and G. Ro, JHEP **08**, 026 (2014), 1403.4953.
- [45] M. Gonderinger, Y. Li, H. Patel, and M. J. Ramsey-Musolf, JHEP **01**, 053 (2010), 0910.3167.
- [46] M. Gonderinger, H. Lim, and M. J. Ramsey-Musolf, Phys. Rev. **D86**, 043511 (2012), 1202.1316.
- [47] W. Chao, M. Gonderinger, and M. J. Ramsey-Musolf, Phys. Rev. **D86**, 113017 (2012), 1210.0491.
- [48] E. Gabrielli, M. Heikinheimo, K. Kannike, A. Racioppi, M. Raidal, and C. Spethmann, Phys. Rev. **D89**, 015017 (2014), 1309.6632.
- [49] P. Ghosh, A. K. Saha, and A. Sil, Phys. Rev. **D97**, 075034 (2018), 1706.04931.
- [50] S. Bhattacharya, P. Ghosh, T. N. Maity, and T. S. Ray, JHEP **10**, 088 (2017), 1706.04699.
- [51] I. Garg, S. Goswami, K. Vishnudath, and N. Khan, Phys. Rev. D **96**, 055020 (2017), 1706.08851.
- [52] A. Dutta Banik, A. K. Saha, and A. Sil, Phys. Rev. **D98**, 075013 (2018), 1806.08080.
- [53] D. Borah, R. Roshan, and A. Sil (2020), 2007.14904.
- [54] L. Lopez Honorez, E. Nezri, J. F. Oliver, and M. H. G. Tytgat, JCAP **0702**, 028 (2007), hep-ph/0612275.
- [55] L. Lopez Honorez and C. E. Yaguna, JHEP **09**, 046 (2010), 1003.3125.
- [56] A. Belyaev, G. Cacciapaglia, I. P. Ivanov, F. Rojas-Abatte, and M. Thomas, Phys. Rev. **D97**, 035011 (2018), 1612.00511.
- [57] S. Choubey and A. Kumar, JHEP **11**, 080 (2017), 1707.06587.
- [58] L. Lopez Honorez and C. E. Yaguna, JCAP **1101**, 002 (2011), 1011.1411.
- [59] A. Ilnicka, M. Krawczyk, and T. Robens, Phys. Rev. **D93**, 055026 (2016), 1508.01671.
- [60] A. Arhrib, Y.-L. S. Tsai, Q. Yuan, and T.-C. Yuan, JCAP **1406**, 030 (2014), 1310.0358.
- [61] Q.-H. Cao, E. Ma, and G. Rajasekaran, Phys. Rev. **D76**, 095011 (2007), 0708.2939.
- [62] E. Lundstrom, M. Gustafsson, and J. Edsjo, Phys. Rev. **D79**, 035013 (2009), 0810.3924.
- [63] M. Gustafsson, S. Rydbeck, L. Lopez-Honorez, and E. Lundstrom, Phys. Rev. **D86**, 075019 (2012), 1206.6316.

- [64] J. Kalinowski, W. Kotlarski, T. Robens, D. Sokolowska, and A. F. Zarnecki, JHEP **12**, 081 (2018), 1809.07712.
- [65] A. Bhardwaj, P. Konar, T. Mandal, and S. Sadhukhan (2019), 1905.04195.
- [66] S. Jangid, P. Bandyopadhyay, P. Bhupal Dev, and A. Kumar, JHEP **08**, 154 (2020), 2001.01764.
- [67] P. Bandyopadhyay, E. J. Chun, and R. Mandal, JCAP **08**, 019 (2020), 2005.13933.
- [68] T. Araki, C. Q. Geng, and K. I. Nagao, Phys. Rev. **D83**, 075014 (2011), 1102.4906.
- [69] O. Fischer and J. J. van der Bij, JCAP **1401**, 032 (2014), 1311.1077.
- [70] N. Khan, Eur. Phys. J. **C78**, 341 (2018), 1610.03178.
- [71] S. Jangid and P. Bandyopadhyay, Eur. Phys. J. C **80**, 715 (2020), 2003.11821.
- [72] C.-W. Chiang, G. Cottin, Y. Du, K. Fuyuto, and M. J. Ramsey-Musolf (2020), 2003.07867.
- [73] D. de Florian et al. (LHC Higgs Cross Section Working Group) (2016), 1610.07922.
- [74] M. Cirelli, N. Fornengo, and A. Strumia, Nucl. Phys. **B753**, 178 (2006), hep-ph/0512090.
- [75] M. Cirelli and A. Strumia, New J. Phys. **11**, 105005 (2009), 0903.3381.
- [76] A. Semenov, Comput. Phys. Commun. **201**, 167 (2016), 1412.5016.
- [77] K. Kannike, Eur. Phys. J. **C72**, 2093 (2012), 1205.3781.
- [78] J. Chakrabortty, P. Konar, and T. Mondal, Phys. Rev. **D89**, 095008 (2014), 1311.5666.
- [79] J. Horejsi and M. Kladiva, Eur. Phys. J. **C46**, 81 (2006), hep-ph/0510154.
- [80] G. Bhattacharyya and D. Das, Pramana **87**, 40 (2016), 1507.06424.
- [81] J. R. Forshaw, D. A. Ross, and B. E. White, JHEP **10**, 007 (2001), hep-ph/0107232.
- [82] C. Cai, Z.-H. Yu, and H.-H. Zhang, Nucl. Phys. B **924**, 128 (2017), 1705.07921.
- [83] S. Yaser Ayazi and S. M. Firouzabadi, JCAP **1411**, 005 (2014), 1408.0654.
- [84] M. Aaboud et al. (ATLAS), Phys. Rev. **D98**, 052005 (2018), 1802.04146.
- [85] A. M. Sirunyan et al. (CMS), Eur. Phys. J. **C79**, 421 (2019), 1809.10733.
- [86] (2004), hep-ex/0412015.
- [87] P. Fileviez Perez, H. H. Patel, M. J. Ramsey-Musolf, and K. Wang, Phys. Rev. D **79**, 055024 (2009), 0811.3957.
- [88] E. Aprile et al. (XENON), Phys. Rev. Lett. **119**, 181301 (2017), 1705.06655.
- [89] S. Yaser Ayazi and S. M. Firouzabadi, Cogent Phys. **2**, 1047559 (2015), 1501.06176.
- [90] P. Athron et al. (GAMBIT), Eur. Phys. J. **C77**, 568 (2017), 1705.07931.
- [91] J. Giedt, A. W. Thomas, and R. D. Young, Phys. Rev. Lett. **103**, 201802 (2009), 0907.4177.

- [92] D. Barducci, G. Belanger, J. Bernon, F. Boudjema, J. Da Silva, S. Kraml, U. Laa, and A. Pukhov, *Comput. Phys. Commun.* **222**, 327 (2018), 1606.03834.
- [93] G. Isidori, G. Ridolfi, and A. Strumia, *Nucl. Phys.* **B609**, 387 (2001), hep-ph/0104016.
- [94] F. Staub, *Comput. Phys. Commun.* **185**, 1773 (2014), 1309.7223.
- [95] C. Coriano, L. Delle Rose, and C. Marzo, *JHEP* **02**, 135 (2016), 1510.02379.
- [96] J. Braathen, M. D. Goodsell, M. E. Krauss, T. Opferkuch, and F. Staub, *Phys. Rev. D* **97**, 015011 (2018), 1711.08460.
- [97] B. W. Lee, C. Quigg, and H. B. Thacker, *Phys. Rev.* **D16**, 1519 (1977).